Supporting Information for:

Reconfiguration of π-Conjugated Superstructures Enabled by Redox-Assisted Assembly

Kaixuan Liu,[a] Arindam Mukhopadhyay,[a] Adam Ashcraft,[a] Chuan Liu,[a] Adam Levy,[a] Patricia Blackwelder,[b,c] and Jean-Hubert Olivier [a]*

[a] Department of Chemistry, University of Miami, Cox Science Center, 1301 Memorial Drive, Coral Gables, FL 33146

[b] Center for Advanced Microscopy (UMCAM), Department of Chemistry, University of Miami, Coral Gables, FL 33146

[c] Marine Geological Sciences, Rosenstiel School of Marine and Atmospheric Science, University of Miami, 4600 Rickenbacker Causeway, Miami, FL 33149

*To whom correspondence may be sent: J.-H. Olivier: jh.olivier@miami.edu

Table of Contents:

1. Materials and Instrumentation

Unless otherwise noted, all chemicals were used as received. Air sensitive compounds were handled in Braun Labmaster DP glove box. *N,N*-Dimethylformamide (DMF) and *N,N*-dimethylacetamide (DMA) were dehydrated by activated molecular sieves.[1] Standard Schlenk techniques were employed to manipulate air-sensitive solutions. Tetrahydrofuran (THF) was distilled from Na/benzophenone, under argon. All NMR solvents were used as received from Cambridge Isotope Laboratories, Inc. Sodium hydroxide, 4-(bromomethyl) benzoate, and 1-(3-aminopropyl)imidazole were purchased from Alfa Aesar. Perylene-3,4,9,10-tetracarboxylic dianhydride was obtained from Acros Organics. Sodium sulfide and triethylamine were purchased from Sigma-Aldrich. Triethylene glycol was purchased from EMD Millipore. *N,N*-Dimethylethylenediamine, 2-bromoethanol, 1,8-diazabicyclo[5.4.0]undec-7-ene (DBU), 4-dimethylaminopyridine and N,N-dimethylacetamide were purchased from Tokyo Chemical Industry. *N*,*N*-Dimethylformamide, methanol, tetrahydrofuran (THF), dichloromethane and sulfuric acid were purchased from VWR. Flash column chromatography was performed on the bench top, using silica gel (VWR, 70-90 μm). NMR spectra were recorded on an Avance Bruker 400 MHz spectrometer. UV-vis-NIR spectra were recorded on a Cary 5000 equipped with a Peltier-controlled heating stage (Versa 20 from Quantum Northwest). IR spectra were recorded on a Perkin Elmer Frontier FTIR. Mass spectra were obtained on a Micro Q-TOF ESI mass spectrometer. Flash chromatography using a Biotage Isolera purification system was utilized. Scanning electron microscope images were recorded with a Philips XL-30 Field Emission SEM at several magnifications. In some cases, elemental analysis (EDS) was performed using an Oxford/Link System. Transmission electron microscope images were acquired with a JEOL 1400-X TEM located at the Miller School of Medicine TEM Core at the University of Miami. In all cases images were digitally collected. TEM grids were purchased from Ted Pella (product number 01824G). Silicon wafers (single side polished; orientation <111>, P-type with boron as dopant) were purchased from University Wafer.

2. Synthetic Procedures for PDI-C_3Im-C_2OH and PDI-TEOAm-C_2OH Building Blocks

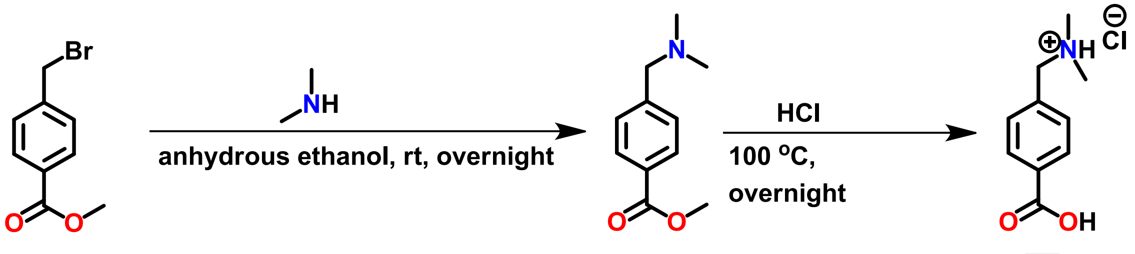

1

2

Carboxylic acid 2:[2] To a solution of methyl 4-(bromomethyl) benzoate (2.3 g, 10 mmol) in 50 mL of anhydrous ethanol at 0 ˚C was added dimethylamine (2 M methanolic solution, 10 mL, 20 mmol). The mixture was stirred at room temperature overnight. The reaction mixture was washed with saturated $NaHCO_3$. The aqueous layer was then extracted with EtOAc and the combined organic layer was washed with brine and dried over anhydrous Na_2SO_4. The solvent was removed under reduced pressure to afford title compound **1** (1.73 g, 89.5%) as a yellow oil. Compound **1** (1.44 g) was dissolved in 100 mL of aq. HCl solution (1 M) and stirred at 100 ˚C overnight. After cooling down to r.t., the solvent was evaporated under reduced pressure to give rise to compound **2** as a white solid (1.58 g, 98%).

Characterization data of **1**. ^{1}H NMR of **1** (400 MHz, $CDCl_3$) δ 8.00 (d, J = 8.1 Hz, 2H), 7.39 (d, J = 8.0 Hz, 2H), 3.91 (s, 3H), 3.47 (s, 2H), 2.25 (s, 6H). ESI-MS$^+$ m/z Calcd for $C_{11}H_{16}NO_2$ 194.1181 $[M+H]^+$, found 194.1190.

Characterization data of **2**. FT-IR (neat solid): $\bar{\upsilon}$ = 3350, 2960, 2675, 1709, 1382, 1230 cm^{-1}. ^{1}H NMR (500 MHz, D_2O) δ 8.00 (dd, J = 8.5 Hz, 2H), 7.54 (dd, J = 8.5 Hz, 2H), 4.33 (d, J = 1.7 Hz, 2H), 2.82 (d, J = 2.0 Hz, 6H).). ESI-MS$^+$ m/z Calcd for $C_{10}H_{14}NO_2$ 180.1025 $[M+H]^+$, found 180.1023.

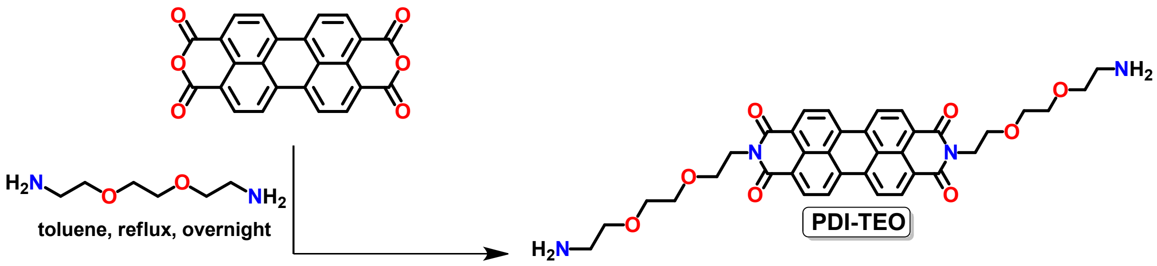

PDI-TEO:[3] To a suspension of 3,4,9,10-perylenetetracarboxylic dianhydride (2 g, 5.1 mmol) in toluene (160 mL) was added 2,2′-(ethylenedioxy)bis(ethylamine) (22 mL, 153 mmol). The mixture was refluxed overnight, cooled down to r.t., filtered, and washed with toluene. The solid, thus obtained, was added to 5 M KOH (100 mL) solution and stirred at r.t. for 6 h. The reaction mixture was filtered and washed with water (pH = 12). The resulting solid was dissolved in the mixture of methanol and chloroform (1:3) and separated by suction filtration. Evaporation of solvent provided a dark red solid (0.9 g, 26.4%).

Characterization data of **PDI-TEO**. FT-IR (neat solid): $\bar{\upsilon}$ = 3210, 3071, 2870, 1687, 1651, 1591, 1334, 1243 cm^{-1}. ^{1}H NMR (500 MHz, $CDCl_3$) δ = 8.69 (d, J = 7.9 Hz, 4H), 8.61 (d, J = 8.1 Hz, 4H) 4.51 (t, J = 5.9 Hz, 4H), 3.91 (t, J = 6.0 Hz, 4H), 3.79-3.74 (m, 4H), 3.66-3.62 (m, 4H), 3.48 (t, J = 5.1 Hz, 4H), 2.81 (t, J = 5.0 Hz, 4H), 1.62 (s, 8H), 1.19 (s, 4H). ESI-MS$^+$ m/z Calcd for $C_{36}H_{37}N_4O_8$ 653.2611 [M+H]$^+$, found 653.2643, Calcd for $C_{36}H_{38}N_4O_8$ 327.1345 [M+2H]$^{2+}$, found 327.1370.

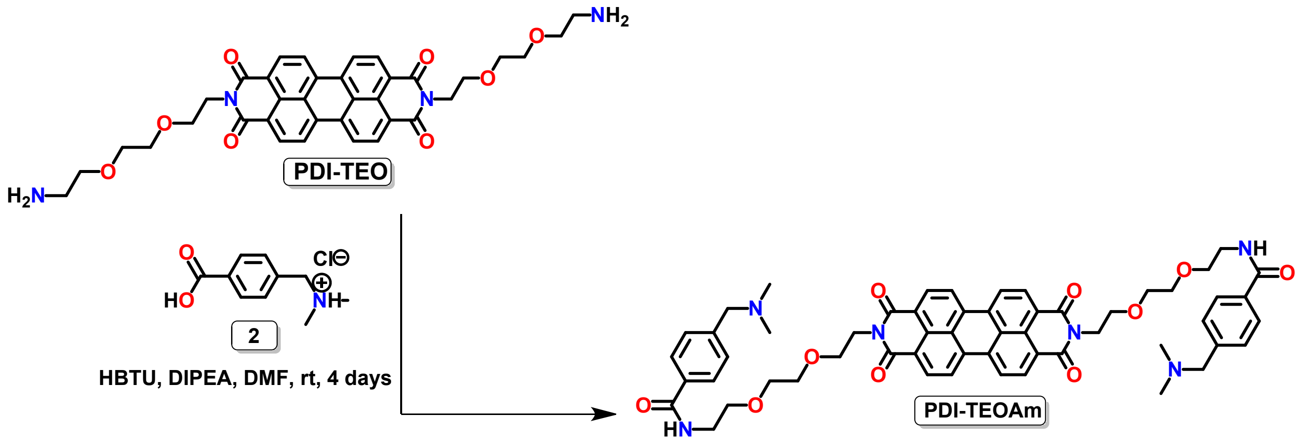

PDI-TEOAm: Carboxylic acid **2** (0.63 g, 4.5 eq) was dissolved in 350 mL of DMF. To this solution were added hexafluorophosphate benzotriazole tetramethyl uronium (HBTU) (1.1 g, 4.5 eq) and DIPEA (2.5 mL, 23 eq) under argon gas atmosphere. After 30 min, **PDI-TEO** (0.4 g, 0.61 mmol) was added to the solution and the reaction mixture was stirred at r.t. for 4 days. The solvent was evaporated under vacuum at 40 ^{o}C, and the resulting solid was purified by flash chromatography using DCM/MeOH/TEA solvent mixture as eluent (gradient elution from 98:1:1 to 94:5:1, *v/v/v*), yielding **PDI-TEOAm** as a red solid (0.251 g, 40.9%).

Characterization data of PDI-TEOAm. FT-IR (neat solid): ῡ = 3292, 3074, 2868, 1691, 1655, 1593, 1338, 1245 cm^{-1}. ^{1}H NMR (400 MHz, $CDCl_3$/MeOD (30:1, *v/v*)) δ 8.66 (d, J = 8.0 Hz, 4H), 8.62 (d, J = 8.4 Hz, 4H), 7.75 (d, J = 8.2 Hz, 4H), 7.35 (d, J = 7.6 Hz, 4H), 4.50 (t, J = 5.7 Hz, 4H), 3.91 (t, J = 5.8 Hz, 4H), 3.76-3.74 (m, 4H), 3.63-3.55 (m, 14H), 3.48 (s, 4H), 2.27 (s, 12H). ESI-MS^{+} m/z Calcd for $C_{56}H_{59}N_6O_{10}$ 975.4293 [M+H]$^{+}$, found 975.4350, Calcd for $C_{56}H_{60}N_6O_{10}$ 488.2186 [M+2H]$^{2+}$, found 488.2230.

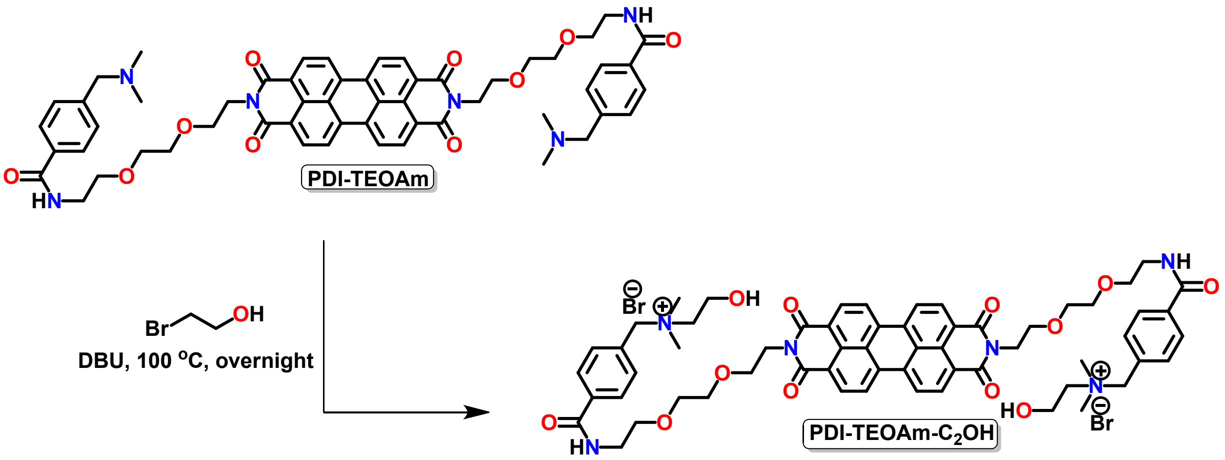

PDI-TEOAm-C$_2$OH: A solution of **PDI-TEOAm** (42 mg, 0.04 mmol), 1,8-diazabicyclo[5.4.0]undec-7-ene (DBU) (0.1 mL, 0.67 mmol) and 2-bromoethanol (0.3 mL, 4.2 mmol) was stirred at 100 ˚C overnight. After cooling down to r.t., 10 mL of THF was added to the reaction mixture and the resulting precipitate was collected by suction filtration and washed with THF (3 * 10 mL). The solid was then dissolved in methanol (~ 20 mL) and gravity-filtered through filter paper. Evaporation of methanol provided the target product (30 mg, 0.024 mmol, 61%).

Characterization data of **PDI-TEOAm-C$_2$OH**. FT-IR (neat solid): $\bar{\upsilon}$ = 3292, 3053, 2924, 1692, 1652, 1594, 1365, 1345 cm^{-1}.^{1}H NMR (400 MHz, d_6-DMSO) δ = 8.62 (t, J = 5.4 Hz, 2H), 8.34 (d, J = 8.0 Hz, 4H,), 8.16 (d, J = 8.3 Hz, 4H), 7.93 (d, J = 7.5 Hz, 4H), 7.62 (d, J = 8.2 Hz, 4H), 5.39-5.33 (m, 2H), 4.63-4.58 (m, 4H), 4.25-4.18 (m, 4H), 3.92-3.89 (m, 4H), 3.73-3.68 (m, 4H), 3.66-3.62 (m, 4H), 3.59-3.57 (m, 4H), 3.55-3.50 (m, 4H), 3.41-3.37(m, 8H), 3.01 (m, 12H). ESI-MS$^+$ m/z Calcd for $C_{60}H_{68}N_6O_{12}$ 532.2448 [M]$^{2+}$, found 532.2457.

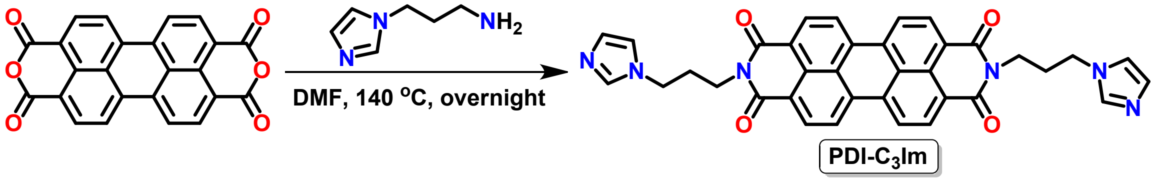

PDI-C$_3$Im:[4] A suspension of 3,4,9,10-perylenetetracarboxylic dianhydride (5 g, 12.7 mmol) and 1-(3-aminopropyl)imidazole (15 mL, 126 mmol) in DMF (100 mL) was stirred overnight at 140 ˚C. After cooling down to r.t., 300 mL of THF was added and the resulting precipitate was collected by suction filtration and washed with THF (3 * 300 mL). Drying under vacuum gave the desired product as a dark red solid (6.7 g, 11 mmol, 92.3%).

Characterization data of **PDI-C$_3$Im**. FT-IR (neat solid): ῡ = 3108, 2963, 2865, 1688, 1646, 1591, 1339, 1246 cm^{-1}. ^{1}H NMR (400 MHz, d_6-DMSO/CF$_3$COOD (30:1, *v/v*)) δ = 9.16 (s, 2H), 8.47 (d, J = 6.6 Hz, 4H), 8.25 (d, J = 7.4 Hz, 4H), 7.84 (s, 2H), 7.73 (s, 2H), 5.15(br, s), 4.34 (t, J = 6.2 Hz, 4H), 4.13-4.03 (m, 4H), 2.37-2.17 (m, 4H). ESI-MS$^+$ m/z Calcd for $C_{36}H_{27}N_6O_4$ 607.2094 [M+H]$^+$, found 607.2075, Calcd for $C_{36}H_{28}N_6O_4$ 304.1086 [M+2H]$^{2+}$, found 304.1083.

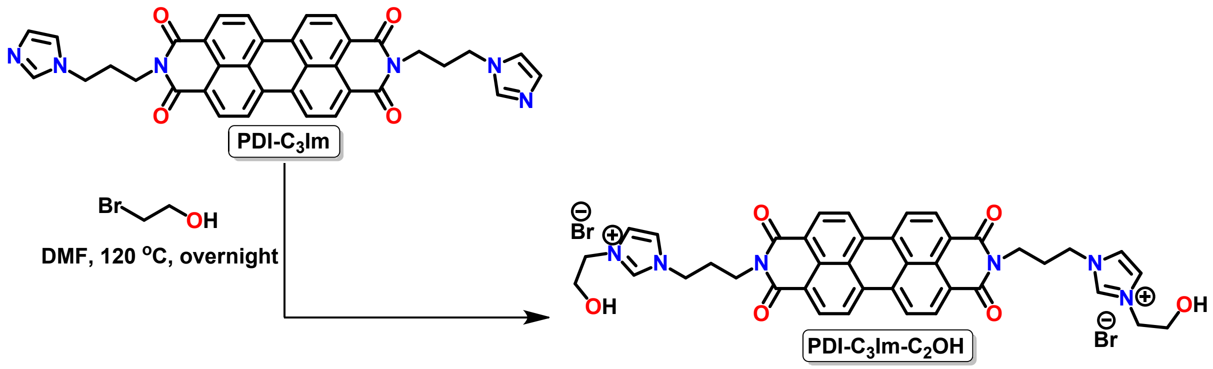

PDI-C$_3$Im-C$_2$OH: A suspension of **PDI-C$_3$Im** (0.5 g, 0.82 mmol), 1,8-diazabicyclo[5.4.0]undec-7-ene (DBU) (0.2 mL, 4.1 mmol) and 2-bromoethanol (10 mL, 141 mmol) was stirred at 100 ˚C overnight. After cooling down to r.t., 100 mL of THF was added to the reaction mixture and the resulting precipitate was collected by suction filtration and washed with THF (2 * 200 mL). The precipitate was dried under vacuum to give a dark red solid (0.61 g, 0.7 mmol, 87%).

Characterization data of **PDI-C$_3$Im-C$_2$OH**. FT-IR: $\bar{\upsilon}$ = 3326, 3143, 1686, 1642, 1592, 1400, 1339, 1249 cm^{-1}. ^{1}H NMR (500 MHz, d_6-DMSO) δ = 9.21 (s, 2H), 8.48 (d, J = 7.9 Hz, 4H), 8.26 (d, J = 7.7 Hz, 4H), 7.86 (s, 2H), 7.80 (s, 2H), 5.19 (br, s, 2H), 4.35 (t, J = 7.3 Hz, 4H), 4.26 (t, J = 4.8 Hz, 4H), 4.12 (m, 4H), 3.79-3.72 (m, 4H), 2.31-2.22 (m, 4H); ^{13}C NMR (101 MHz, d_6-DMSO) δ = 163.16, 136.91, 133.68, 130.84, 128.23, 125.04, 124.32, 123.32, 122.44, 59.75, 52.18, 47.42, 37.36, 28.93. ESI-MS$^+$ m/z Calcd for $C_{40}H_{36}N_6O_6$ 348.1348 [M]$^{2+}$, found 348.1372.

3. Supramolecular Polymerization

The fraction of aggregated molecules (α_{agg}) at a given temperature can be calculated from equation S1:[5]

$$\alpha_{agg} = 1 - \left(\frac{\varepsilon(t) - \varepsilon(agg)}{\varepsilon(mono) - \varepsilon(agg)}\right) \qquad \text{(S1)}$$

Where ε(mono) and ε(agg) stand for the extinction coefficient of the monomer and the fully aggregated state respectively, and ε(t) represents the extinction coefficient at the given temperature (t).

The fraction of aggregated species (α_{agg}) as a function of temperature can be fitted using non-linear least squares regression method based on equation S2:[6]

$$\alpha_{agg} = 1 - \frac{1}{1 + exp(-0.908\,\Delta H\,\frac{T - Tm}{R\,Tm})} \qquad \text{(S2)}$$

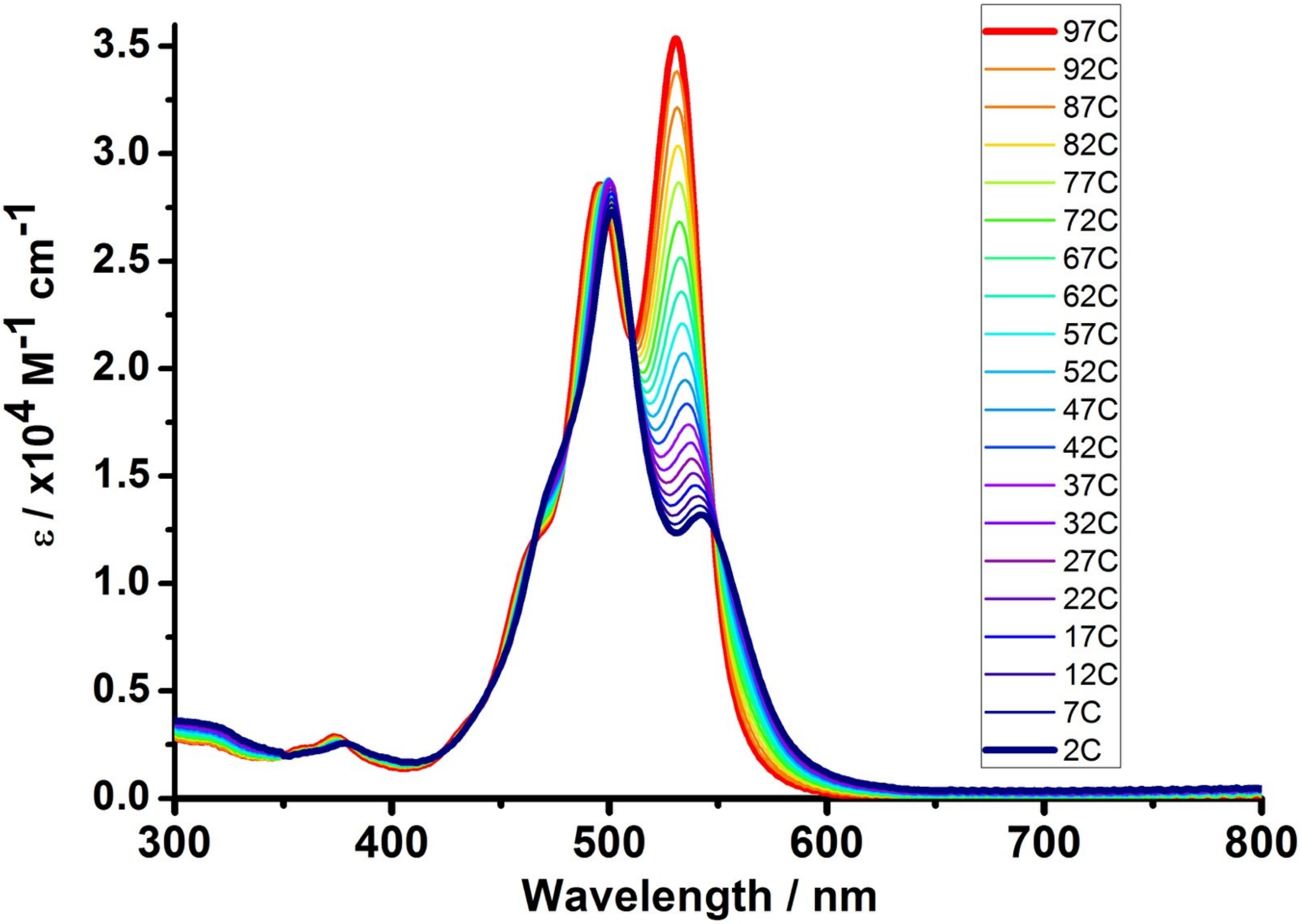

Figure S1. Temperature-dependent UV-vis spectra of **PDI-C_3Im-C_2OH** (5 μM in H_2O solution) recorded between 370 K and 275 K at 5 K intervals. Ramping rate: 1 K/min.

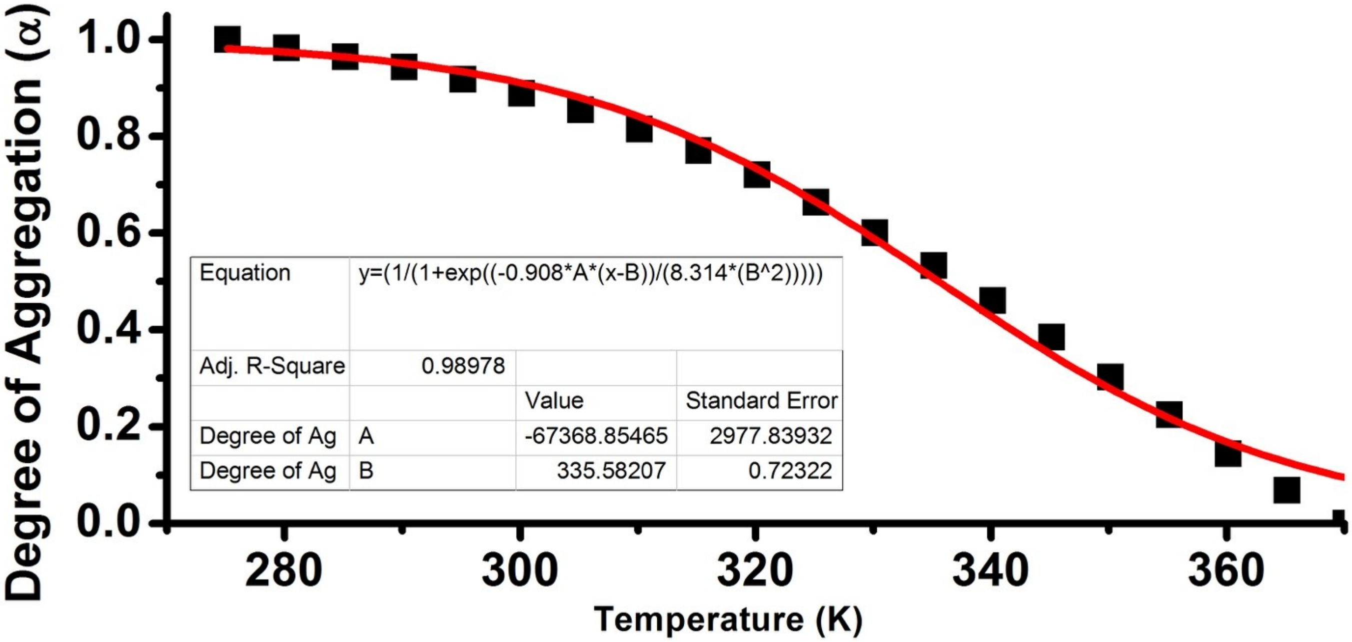

Equation	y=(1/(1+exp((-0.908*A*(x-B))/(8.314*(B^2)))))		
Adj. R-Square	0.98978		
		Value	Standard Error
Degree of Ag	A	-67368.85465	2977.83932
Degree of Ag	B	335.58207	0.72322

Figure S2. Temperature-dependent degree of aggregation, α, calculated from the change extinction coefficient at 530 nm measured from Figure S1. Data were fitted using the isodesmic supramolecular polymerization model.

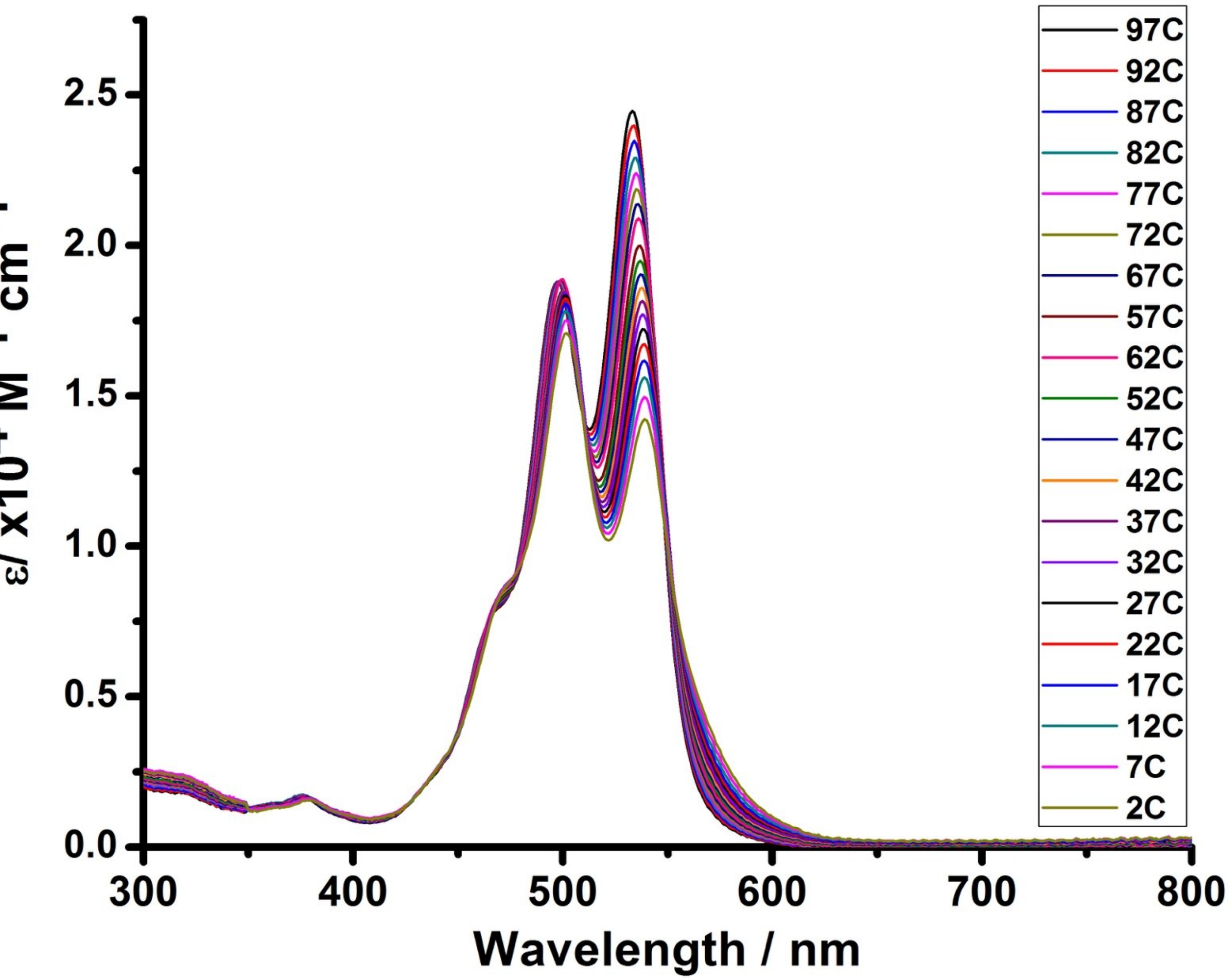

Figure S3. UV-vis spectra of **PDI-TEOAm-C$_2$OH** in H_2O recorded between 370 K and 275 K at 5 K intervals. Ramping rate: 1 K/min.

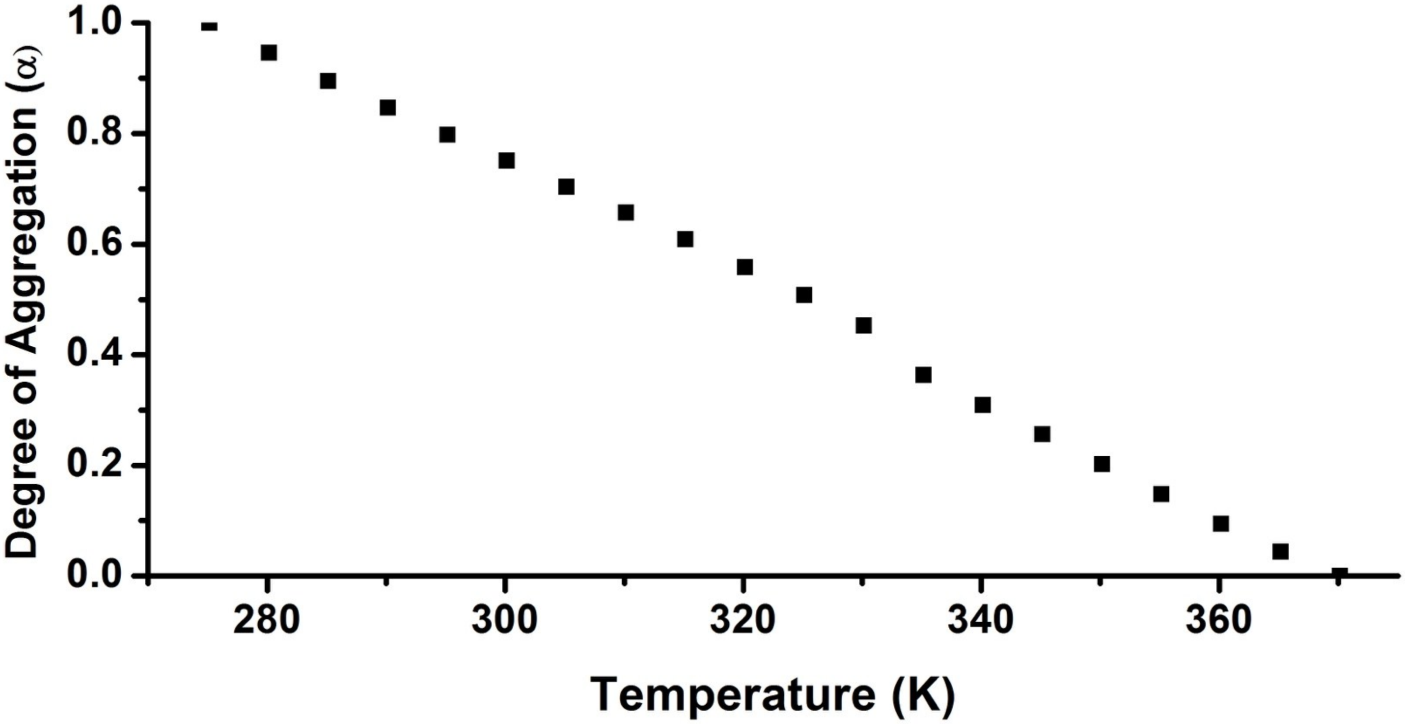

Figure S4. Temperature-dependent aggregation of **PDI-TEOAm-C_2OH (**5μM in H_2O solution) recorded between 370 K and 275 K at 5 K intervals.

To elucidate supramolecular polymerization mechanism, the investigated building blocks should exist as fully aggregated at low temperature and as monomeric species at high temperature. While at 371 K **PDI-TEOAm-C_2OH** building-block exists primarily as molecularly dissolved species, the absorption profile at 275 K suggests that it is not fully aggregated. As shown in Figure S4 that chronicles the degree of aggregation of **PDI-TEOAm-C_2OH** building blocks as a function of temperature, the linear relationship suggests that the entire supramolecular polymerization process cannot be captured using **PDI-TEOAm-C_2OH** building blocks.

4. Reductive Titration Experiments and Control Samples

Redox-Treated Superstructures. A solution of 500 µL of initially prepared **PDI-C_3Im-C_2OH** or **PDI-TEOAm-C_2OH** assemblies in D_2O (concentration range from 0.19 to 0.2 mM) was placed in a 2 mm spectroscopic cell and was further degassed under a gentle flow of argon over 10 min. To this solution was added a total of 200 µL of a D_2O solution of Na_2S (Solution 1, concentration = 1.0 mM, 2 eq. with respect to initial building blocks concentration) in an incremental fashion (10 µL, corresponding to 0.1 eq. of building block) and the corresponding electronic absorption spectrum after each addition was recorded at 20 °C. Subsequently, 10 µL of a D_2O solution of Na_2S (Solution 2, concentration = 30.0 mM, 5 eq. with respect to initial building blocks concentration) was added into the resultant solution and the final electronic absorption spectrum was recorded at 20 °C. Note that during titration, the color gradually evolves from red (neutral state) to dark blue (n-doped intermediate). Upon exposure to ambient atmosphere by opening the spectroscopic cell to let ambient oxygen diffuse over 10 min, the reduced assemblies were oxidized back to neutral ground-state to yield corresponding redox-treated **PDI-TEOAm-C_2OH** and **PDI-C_3Im-C_2OH** assemblies. Note that to assist diffusion of ambient oxygen, the cell was shaken vigorously. The redox-treated assemblies were eventually allowed to age overnight at 20 °C to form the corresponding superstructures.

Control Samples. To ensure that the increase of exciton bandwidth and the hierarchical superstructures observed for redox-treated **PDI-C_3Im-C_2OH** superstructure was not caused by the change of solution ionic strength during reductive titration, control samples were made as the following: The initial solution of NaSH reductant used to form redox-treated was exposed to air to fully oxidize NaSH into Na_2SO_3 and Na_2SO_4. To ensure total oxidation of NaSH, heat was applied to the solution and the final concentration was adjusted to match the initial salt concentration before the heating step. To a solution of initially prepared **PDI-C_3Im-C_2OH** assemblies was added a solution of oxidized NaSH which mimics the volume and concentration of those used during redox-assisted self-assembly. The resulting solution mixture was allowed to age over 18 hours.

Remarks regarding the use of sodium hydrosulfide as a chemical reductant: While sodium sulfide was used as a reductant, the active, chemical reductive species in aqueous media is NaSH. When dissolved in pH neutral aqueous solution, sodium sulfide reacts with water following:

$$Na_2S + H_2O \longrightarrow NaSH + NaOH$$

To gain further insights into the increase of pH of the analytes as a function of reductant addition, Figure S5 shows the evolution of pH as a function of the number of equivalents of reductant added.

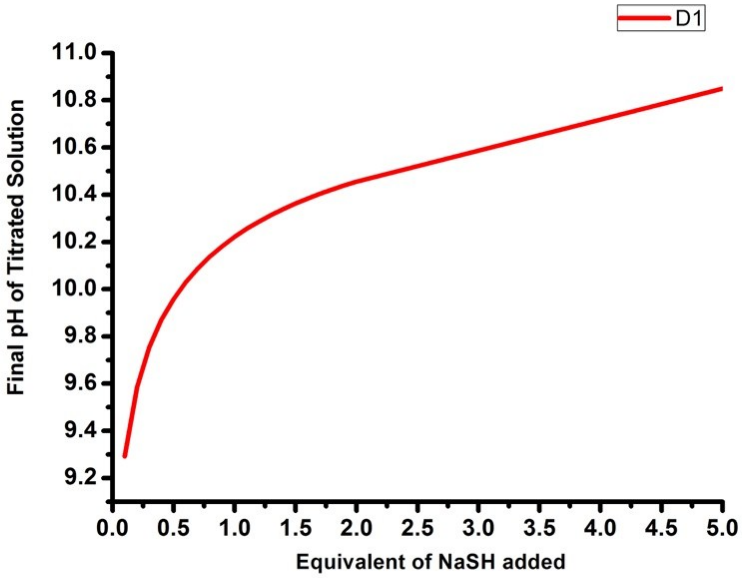

Figure S5. Evolution of the pH of the titrated PDI solutions (**PDI-TEOAm-C_2OH** or **PDI-C_3Im-C2OH**) as a function of the amount of reductant added.

It is important to note that the pH of the analyte remains under basic condition at any given titration point. According to the Sulfur Pourbaix Diagram that chronicles redox potentials as a function of pH, sodium hydrosulfide possesses the necessary redox potential to reduce PDI building blocks.

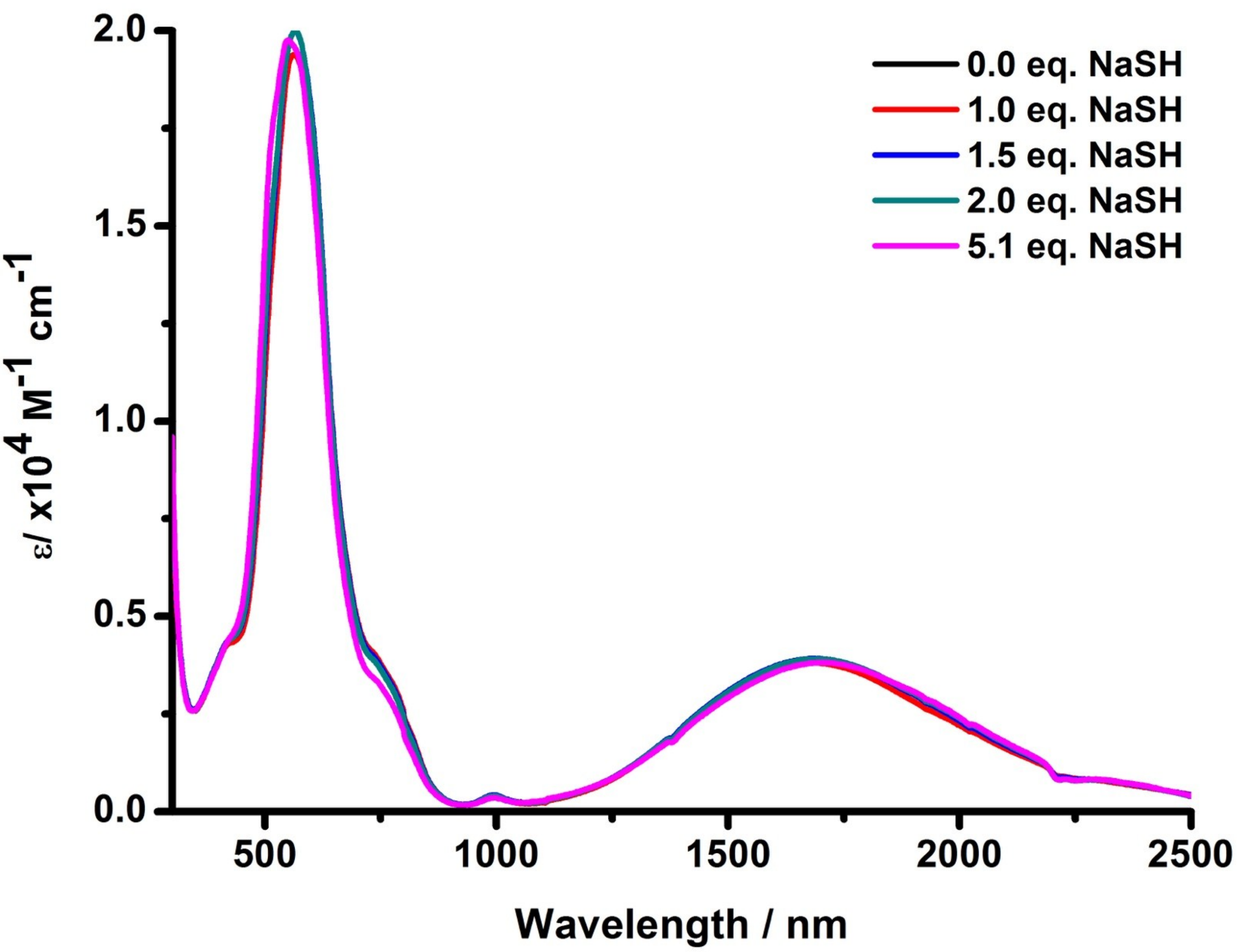

Figure S6. Ground-state electronic absorption spectra recorded in D_2O for non-covalent **PDI-C_3Im-C_2OH** assemblies upon the addition of sodium hydrosulfide (NaSH). Experimental conditions: initial [PDI] = 200 μM; final [PDI] = 140 μM; T = 20˚C; Argon atmosphere, optical pathlength = 2 mm; initial pH = 7.00; final pH = 10.85.

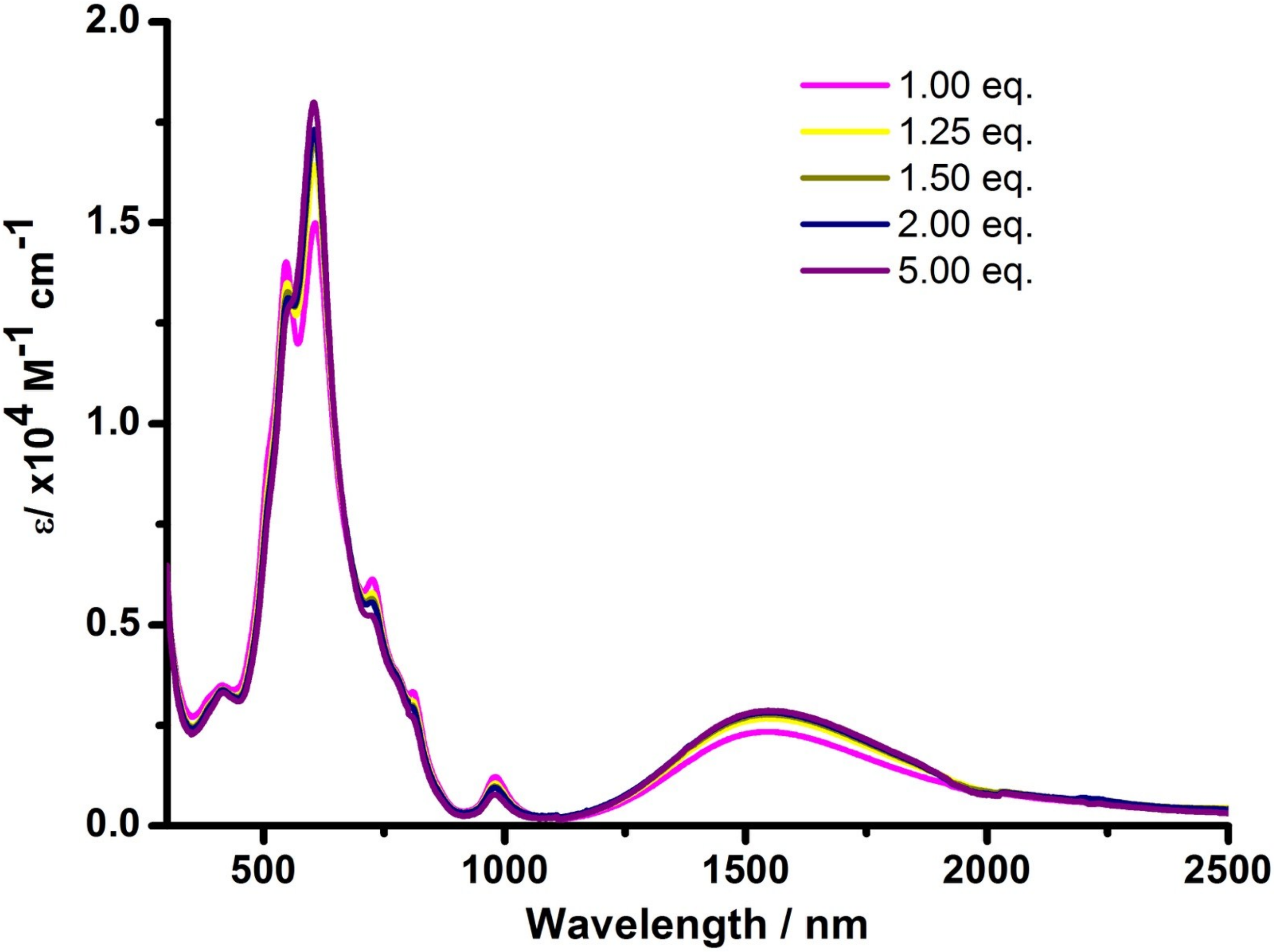

Figure S7. Ground-state electronic absorption spectra recorded in D_2O for non-covalent **PDI-TEOAm-C$_2$OH** assemblies upon the addition of sodium hydrosulfide (NaSH). Experimental conditions: initial [PDI] = 200 µM; final [PDI] = 140 µM; T = 20˚C; Argon atmosphere, optical pathlength = 2 mm; initial pH =7.00; final pH = 10.85.

5. Calculation of the Free-Exciton Bandwidth (Ex_{BW})

Theoretical model developed for H-aggregates in semiconducting polymers was utilized and is shown in equation S1.[7-8] Please note that the Huang-Rhys factor has been calculated from Figure S1 ($\lambda^2 = 0.73$).

$$\frac{I_A^{0-0}}{I_A^{0-1}} \approx \left(\frac{1 - \frac{0.214W}{\hbar\omega_0}}{0.85\left(1 + \frac{0.168W}{\hbar\omega_0}\right)} \right)^2 \qquad (S3)$$

Where I_A^{0-0} and I_A^{0-1} correspond to the oscillator strength of the first two vibronic transitions 0,0 and 0,1 respectively; W corresponds to the free-exciton bandwidth (Ex_{BW}); and $\hbar\omega_0$ is the energy associated to a symmetric ring-stretching mode (180 meV). Oscillator strengths of the 0,0 and 0,1 vibrionic transitions calculated from deconvoluted spectrum shown in Figure 2 have been exploited to calculate the free-exciton bandwidth. The results are presented in Table 1.

Table 1: Oscillator strengths and free-exciton bandwidth Ex_{BW} calculated for initially prepared and redox treated superstructures.

Building Block		**Oscillator Strength**		**Ex_{BW}**
		0,0	0,1	
PDI-C_3Im-C_2OH	Initially Prepared Assembly	0.067	0.204	308 meV
	Redox-Treated Assembly	0.033	0.131	360 meV
PDI-TEOAm-C_2OH	Initially Prepared Assembly	0.0682	0.096	153 meV
	Redox-Treated Assembly	0.0687	0.099	156 meV

6. Scanning and Transmission Electron Microscopic Characterization

TEM samples were prepared by drop casting a solution of initially prepared and redox treated assemblies on a ultrathin carbon film supported by a lacey carbon film on a 300 Mesh Gold Grid (Ted Pella). Strength of the electron beam used: 80kV.

SEM samples were prepared by drop casting a solution of initially prepared and redox treated assemblies on an untreated silicon chip.

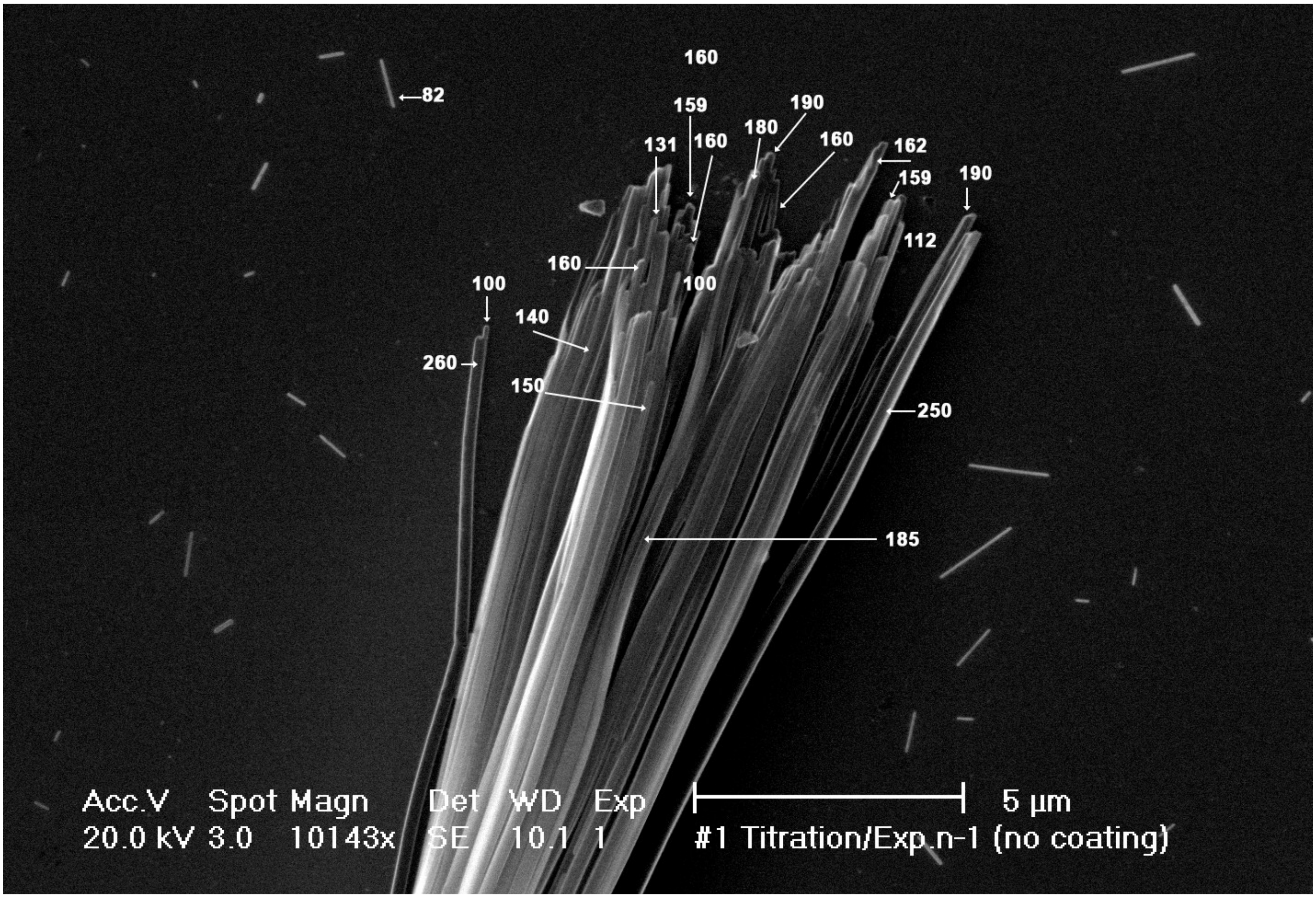

Figure S8. Scanning electron microscopy image of **PDI-C_3Im-C_2OH** superstructure after redox treatment drop casted on a silicon solid-state substrate from parent H_2O solution.

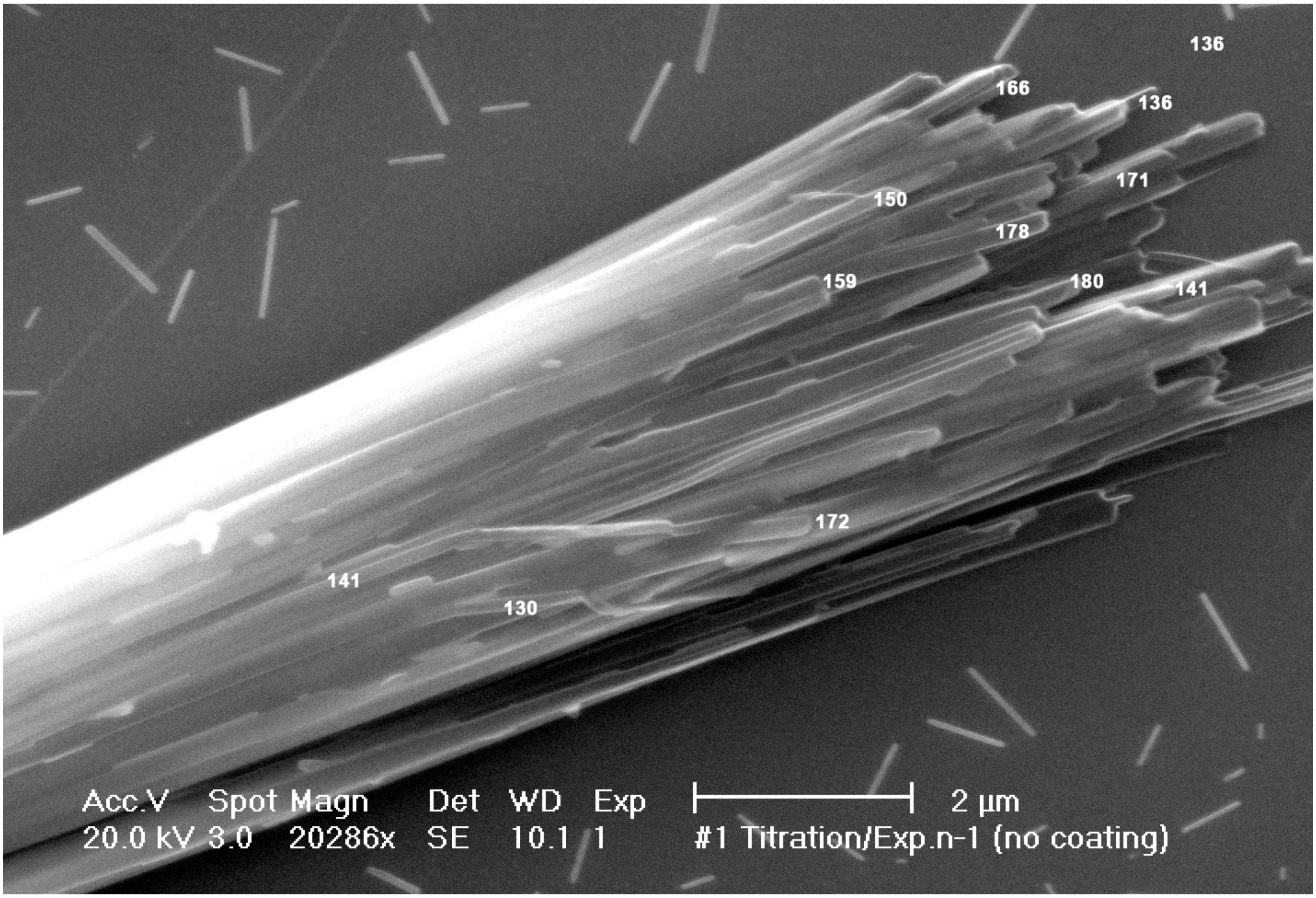

Figure S9. Scanning electron microscopy image of **PDI-C_3Im-C_2OH** superstructure after redox treatment drop casted on a silicon solid-state substrate from parent H_2O solution.

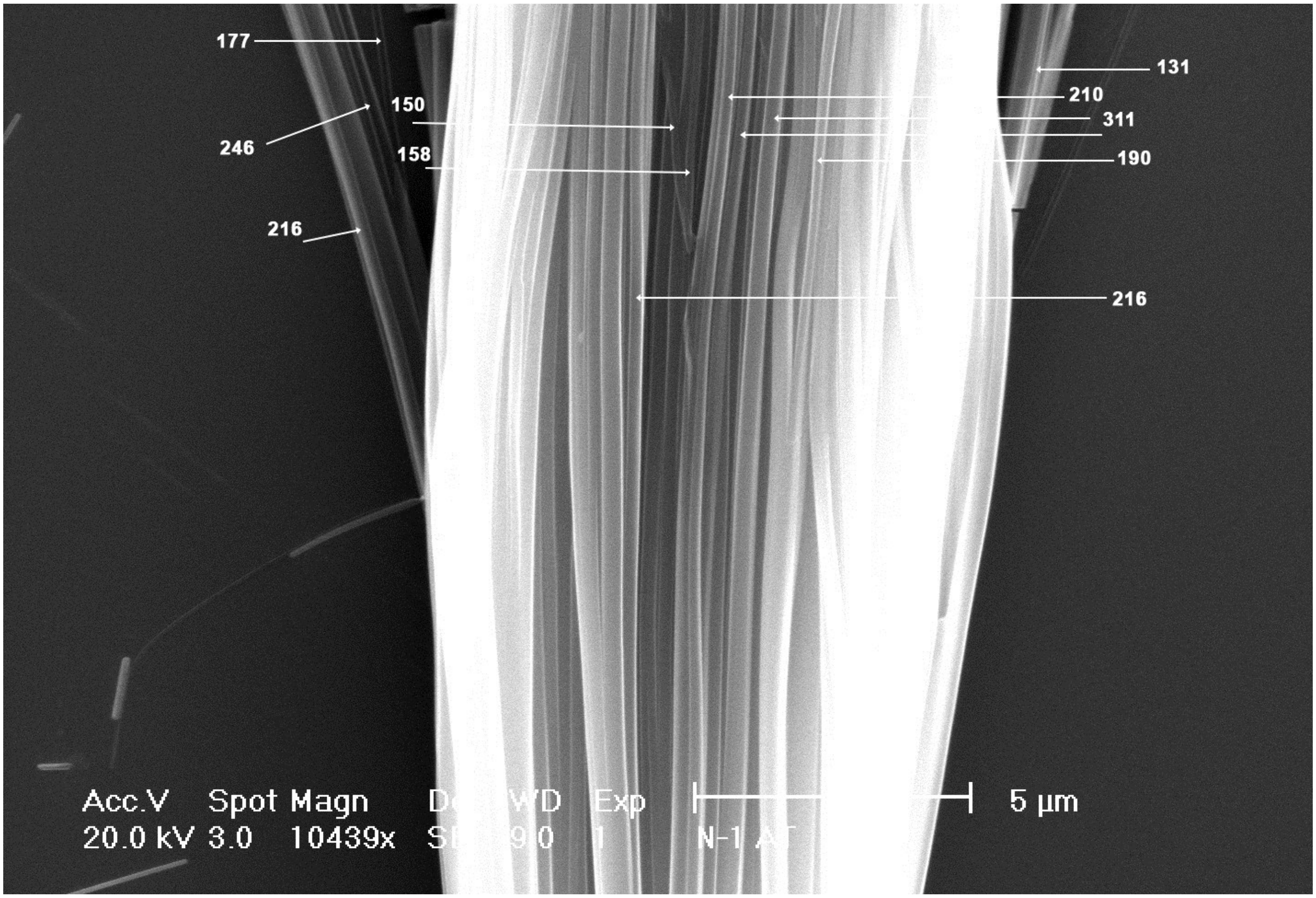

Figure S10. Scanning electron microscopy image of **PDI-C_3Im-C_2OH** superstructure after redox treatment drop casted on a silicon solid-state substrate from parent H_2O solution.

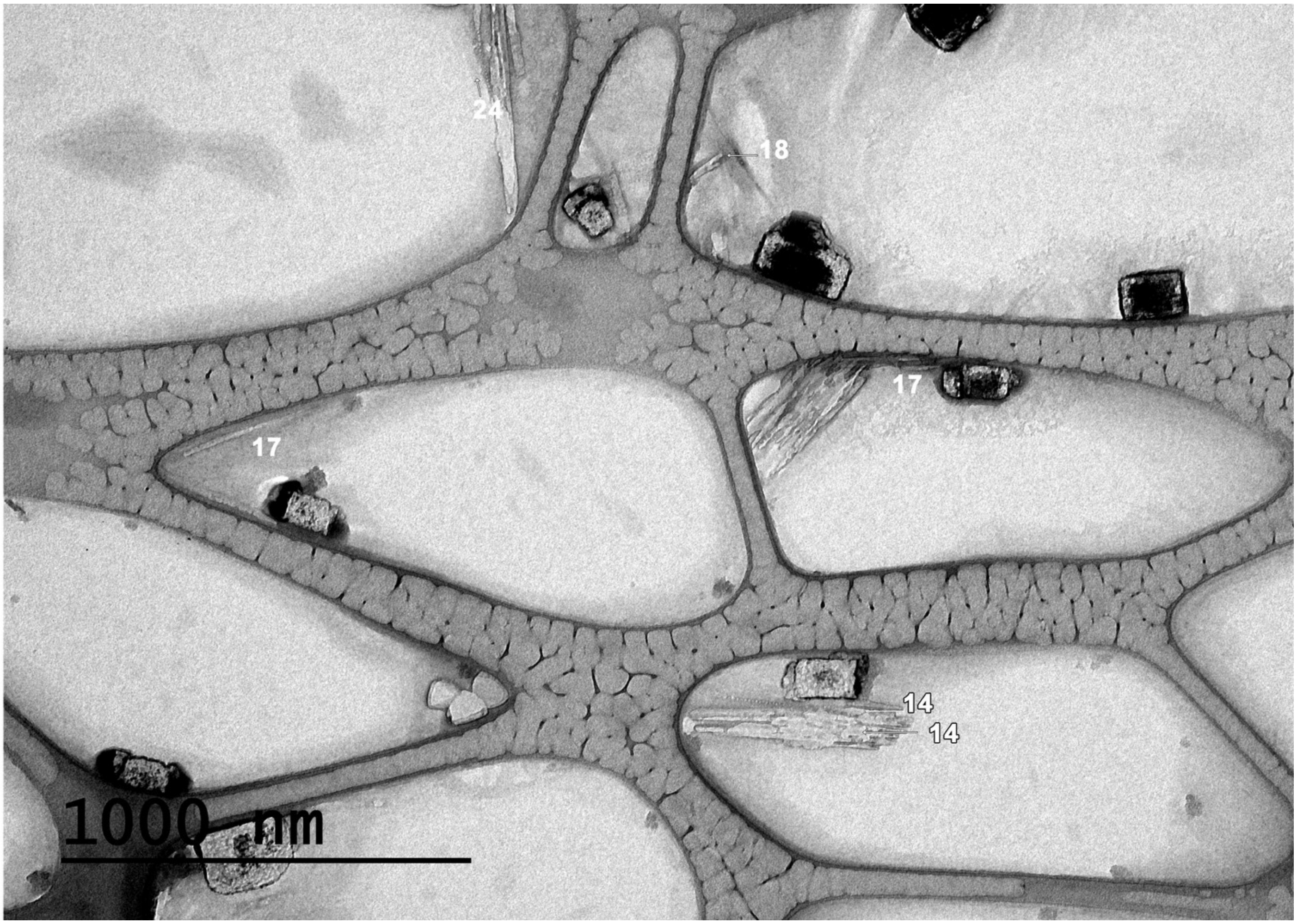

Figure S11. Transmission electron microscopy image of **PDI-C_3Im-C_2OH** superstructure after redox treatment drop casted on a carbon-coated lacey grid from parent H_2O solution.

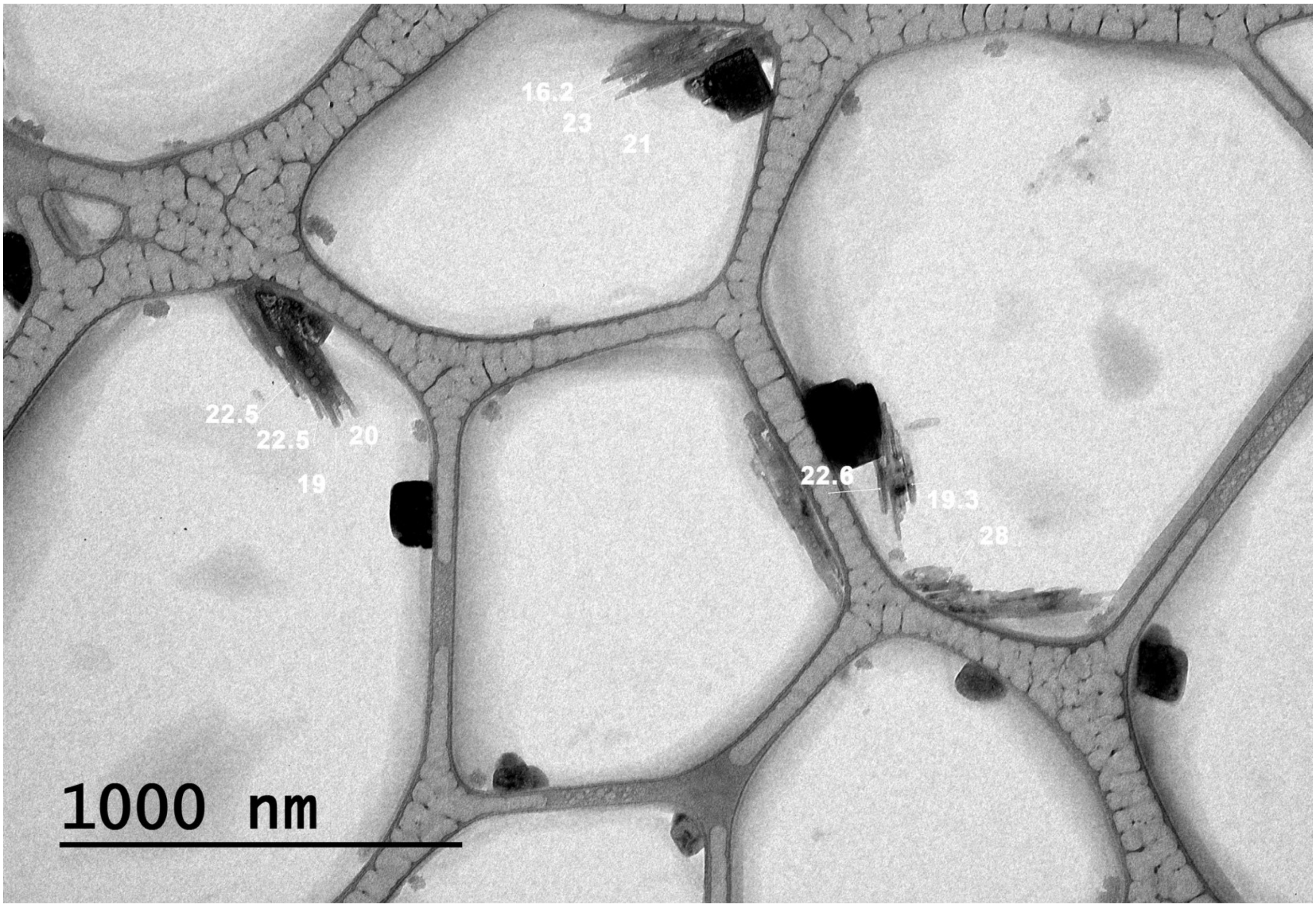

Figure S12. Transmission electron microscopy image of **PDI-C_3Im-C_2OH** superstructure after redox treatment drop casted on a carbon-coated lacey grid from parent H_2O solution.

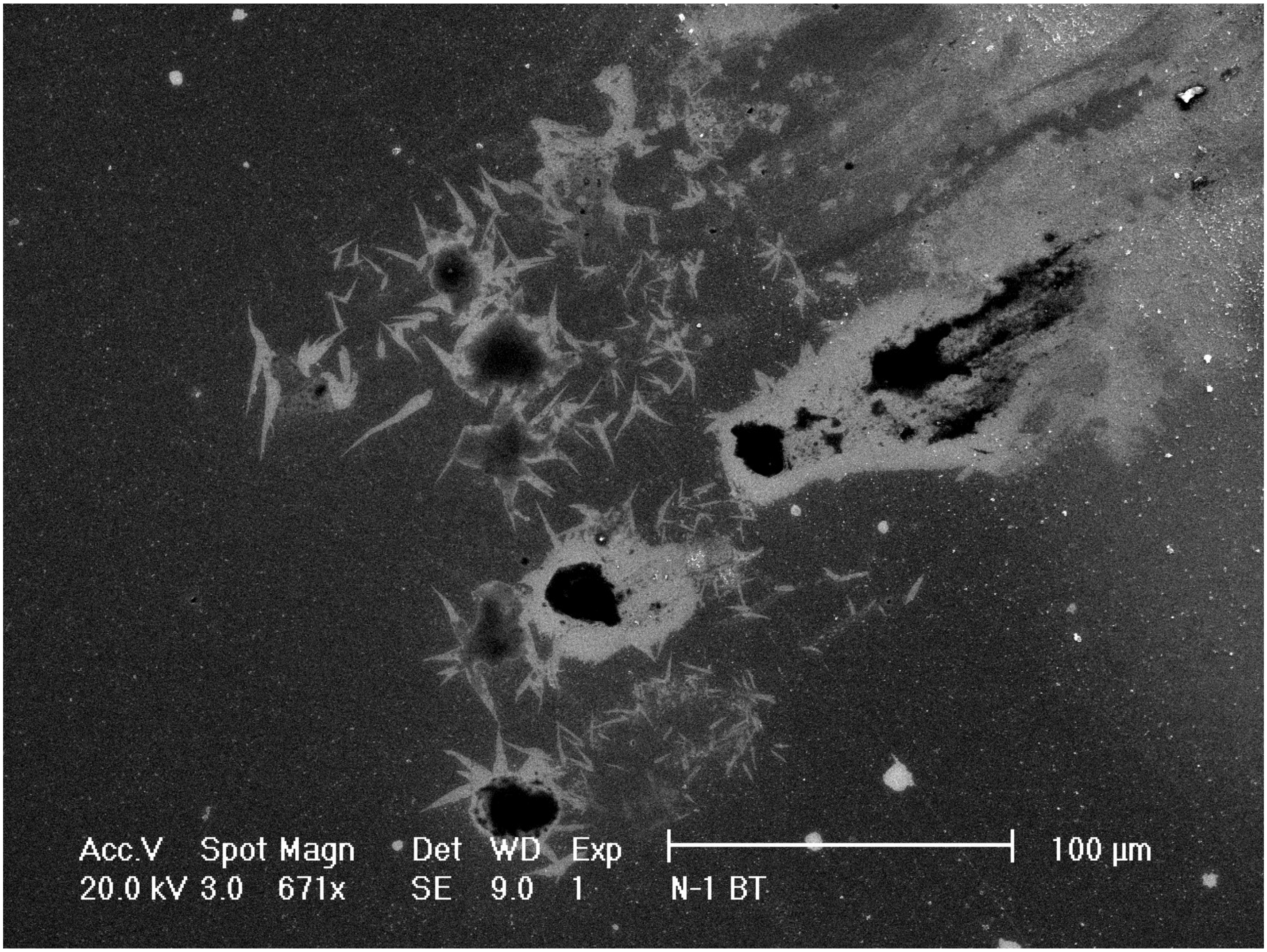

Figure S13. Scanning electron microscopy image of initially prepared **PDI-C_3Im-C_2OH** assembly drop casted on a silicon solid-state substrate from H_2O solution.

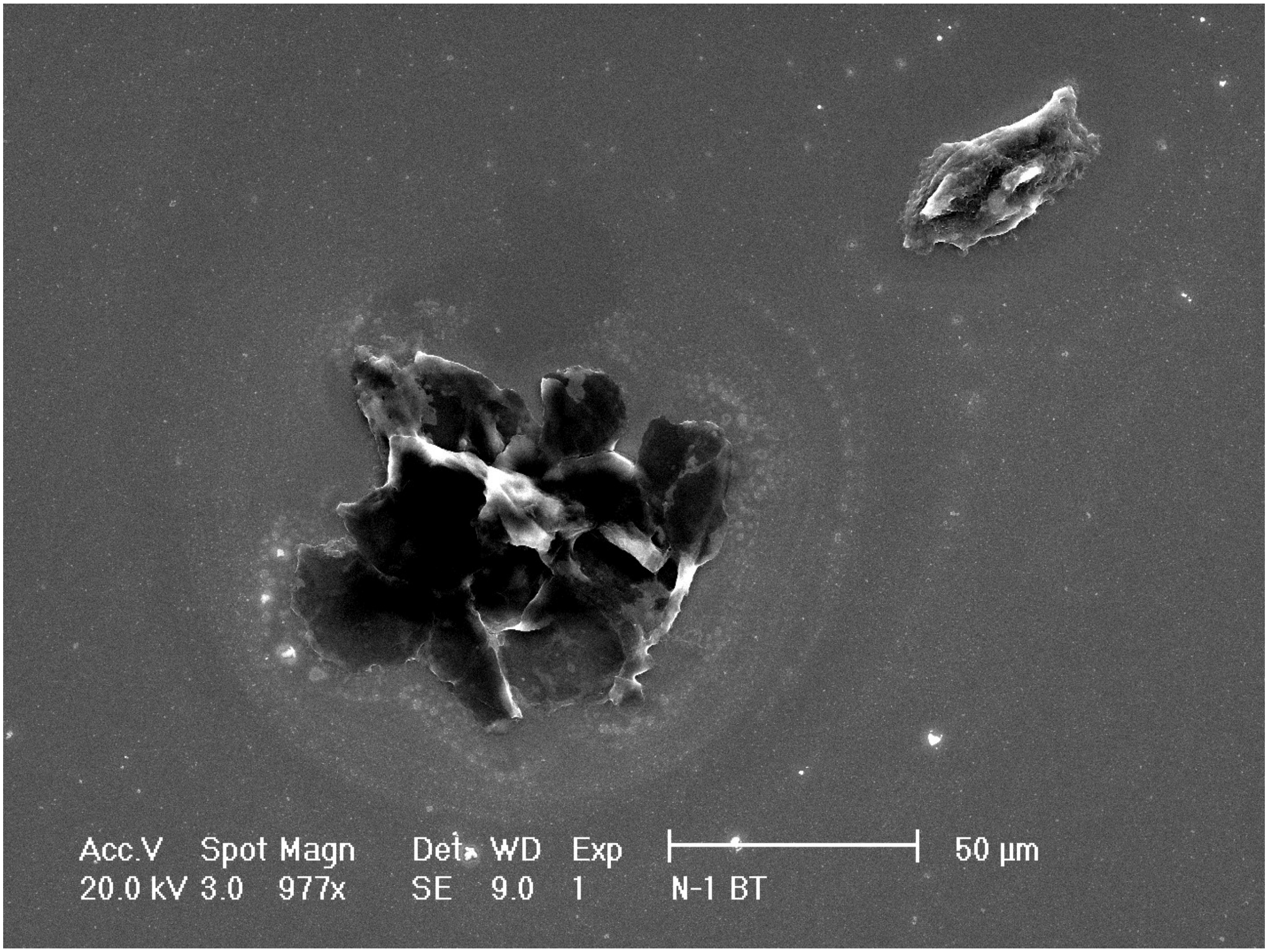

Figure S14. Scanning electron microscopy image of initially prepared **PDI-C_3Im-C_2OH** assembly drop casted on a silicon solid-state substrate from H_2O solution.

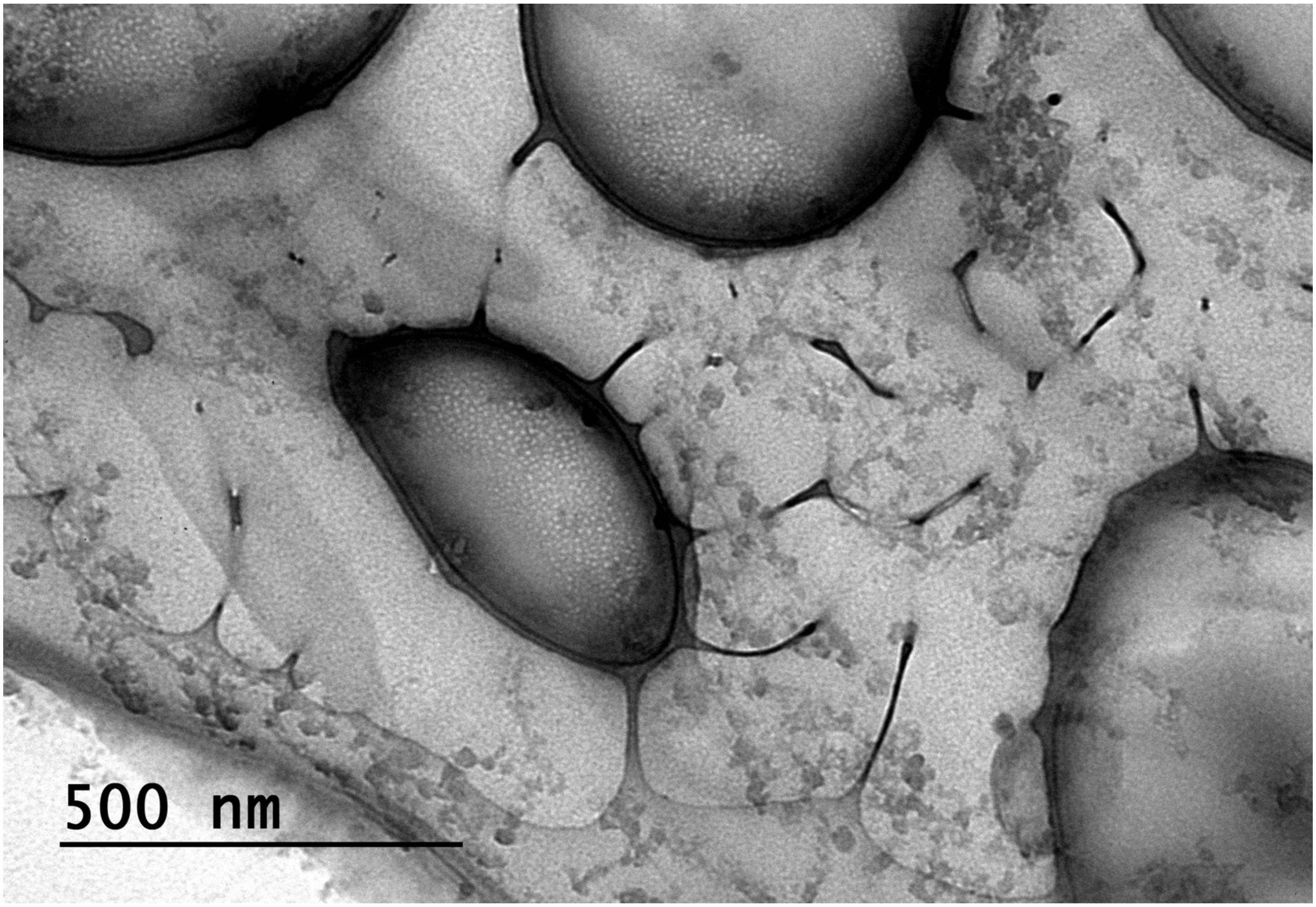

Figure S15. Transmission electron microscopy image of initially prepared **PDI-C_3Im-C_2OH** assembly drop casted on a carbon-coated lacey grid from H_2O solution.

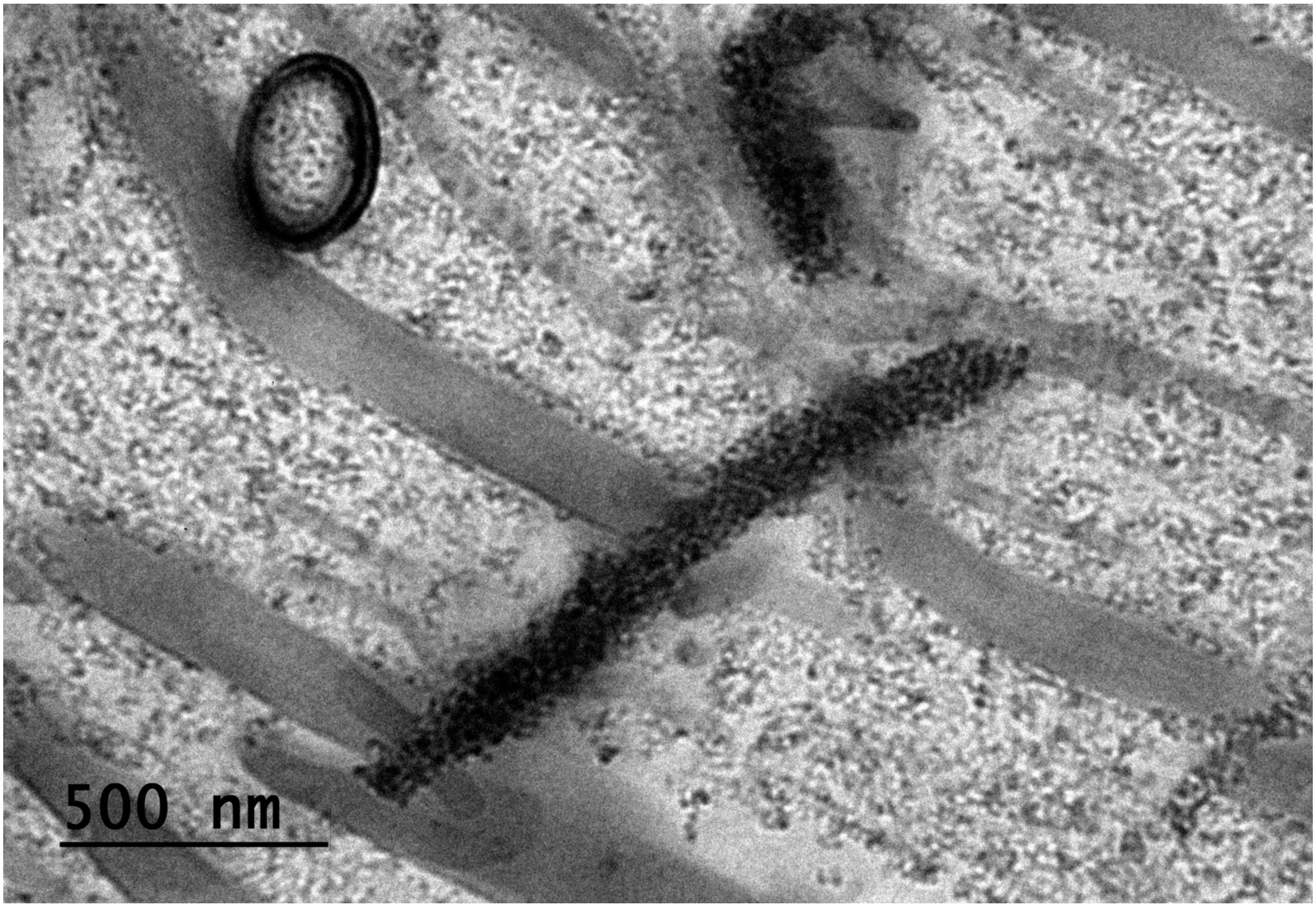

Figure S16. Transmission electron microscopy image of initially prepared **PDI-C_3Im-C_2OH** assembly drop casted on a carbon-coated lacey grid from H_2O solution.

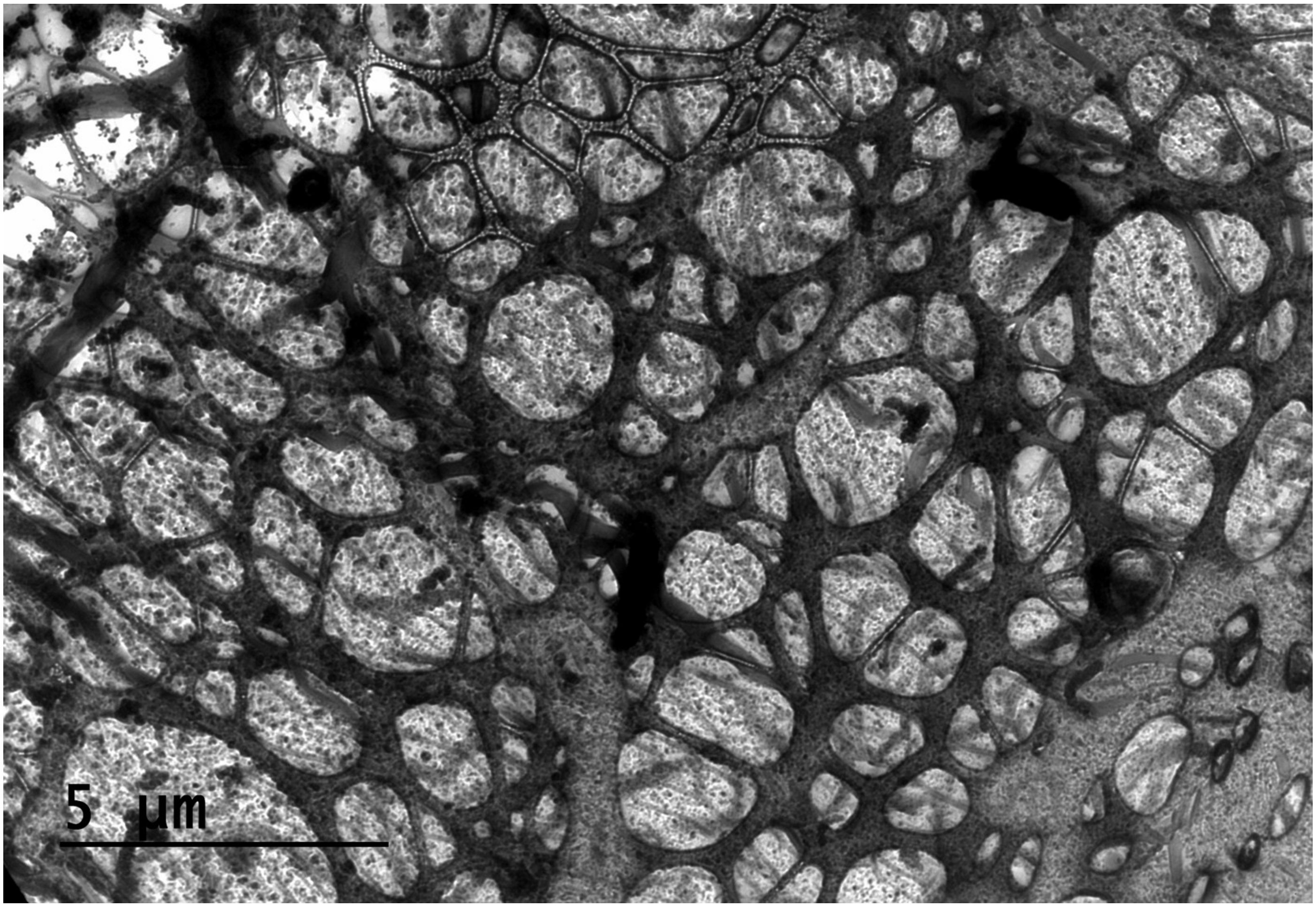

Figure S17. Transmission electron microscopy image of initially prepared **PDI-C_3Im-C_2OH** assembly drop casted on a carbon-coated lacey grid from H_2O solution.

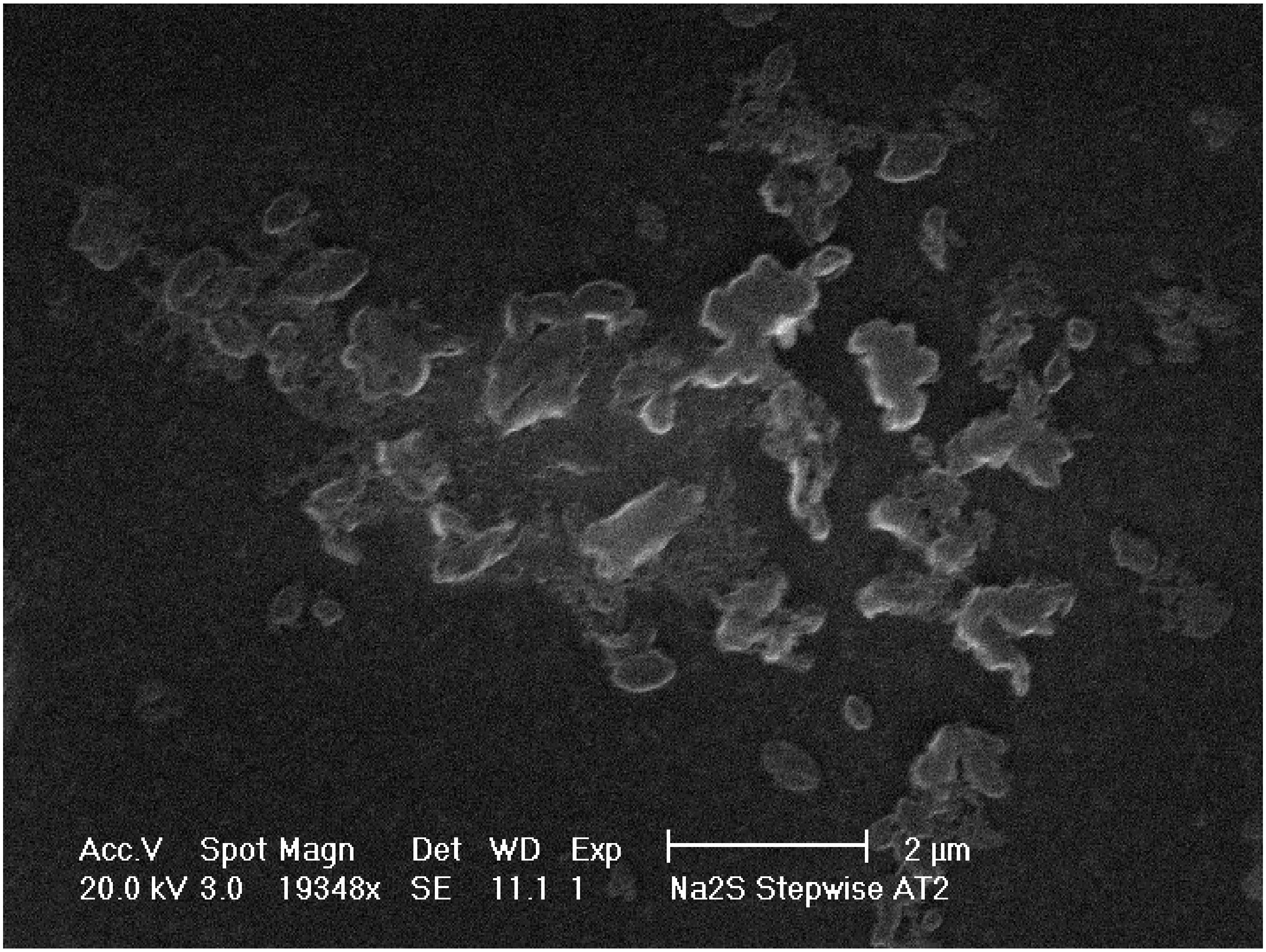

Figure S18. Scanning electron microscopy image of **PDI-TEOAm-C_2OH** superstructure after redox treatment drop casted on a silicon solid-state substrate from parent H_2O solution.

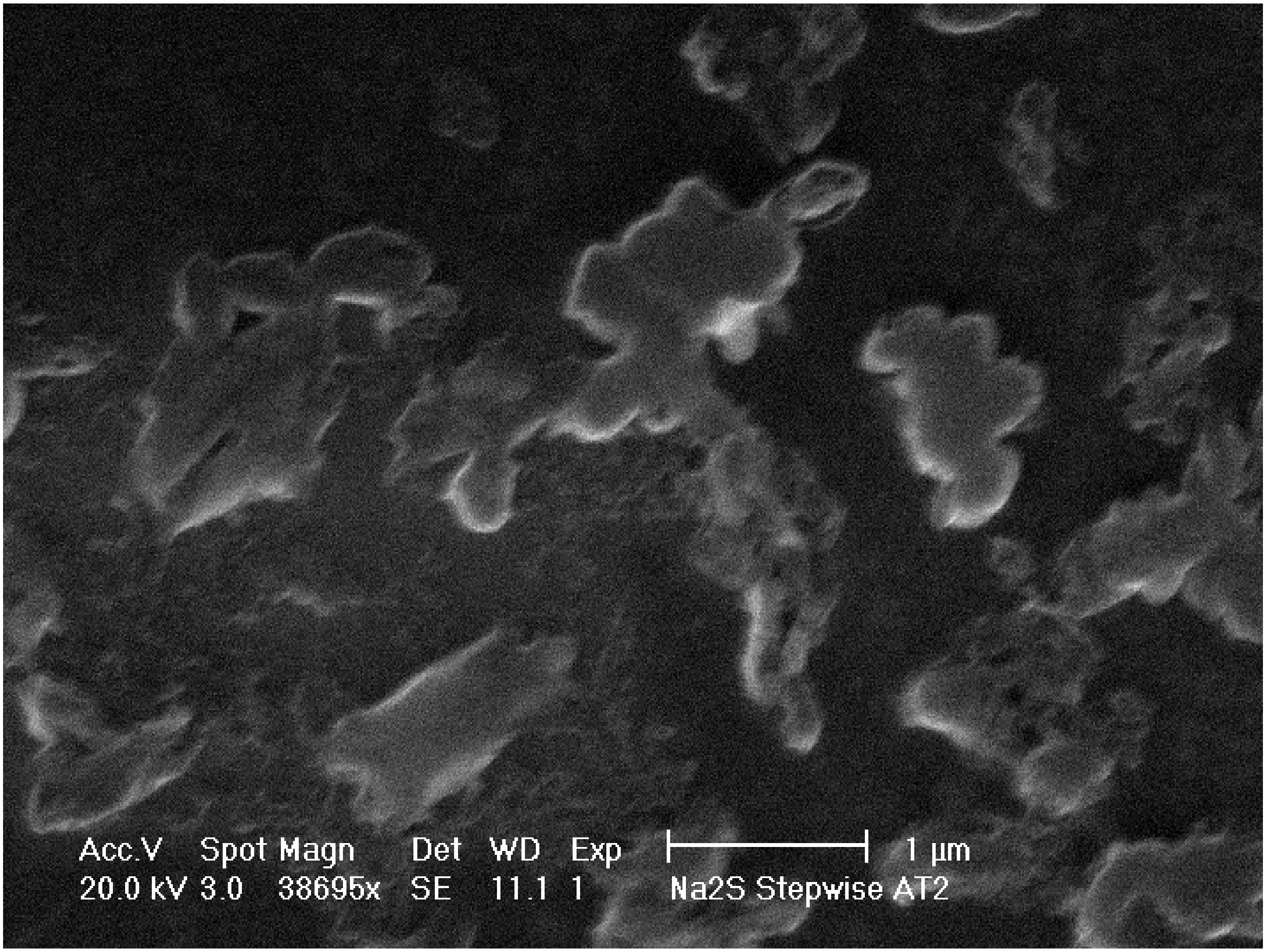

Figure S19. Scanning electron microscopy image of **PDI-TEOAm-C_2OH** superstructure after redox treatment drop casted on a silicon solid-state substrate from parent H_2O solution.

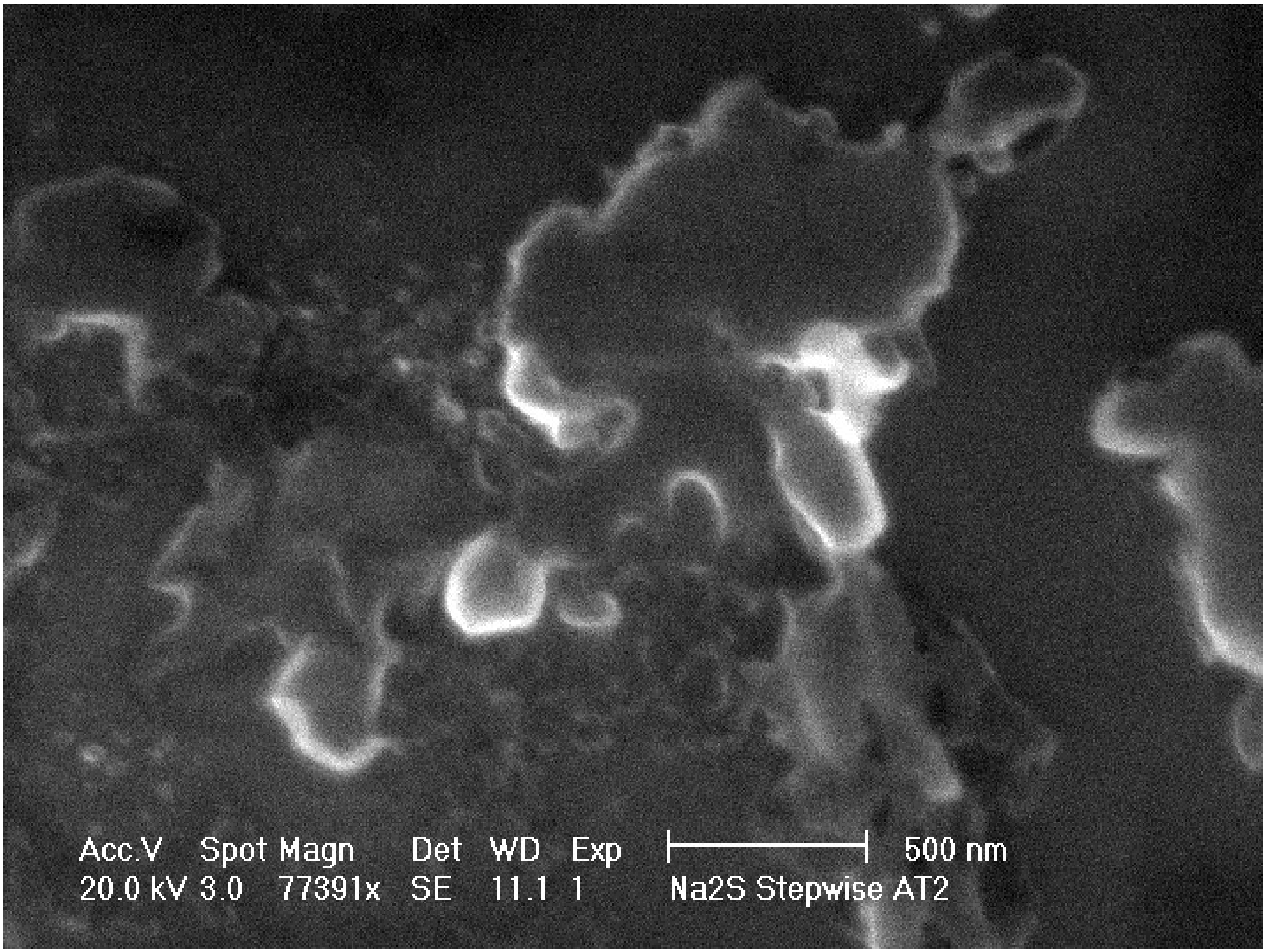

Figure 20. Scanning electron microscopy image of **PDI-TEOAm-C_2OH** superstructure after redox treatment drop casted on a silicon solid-state substrate from parent H_2O solution.

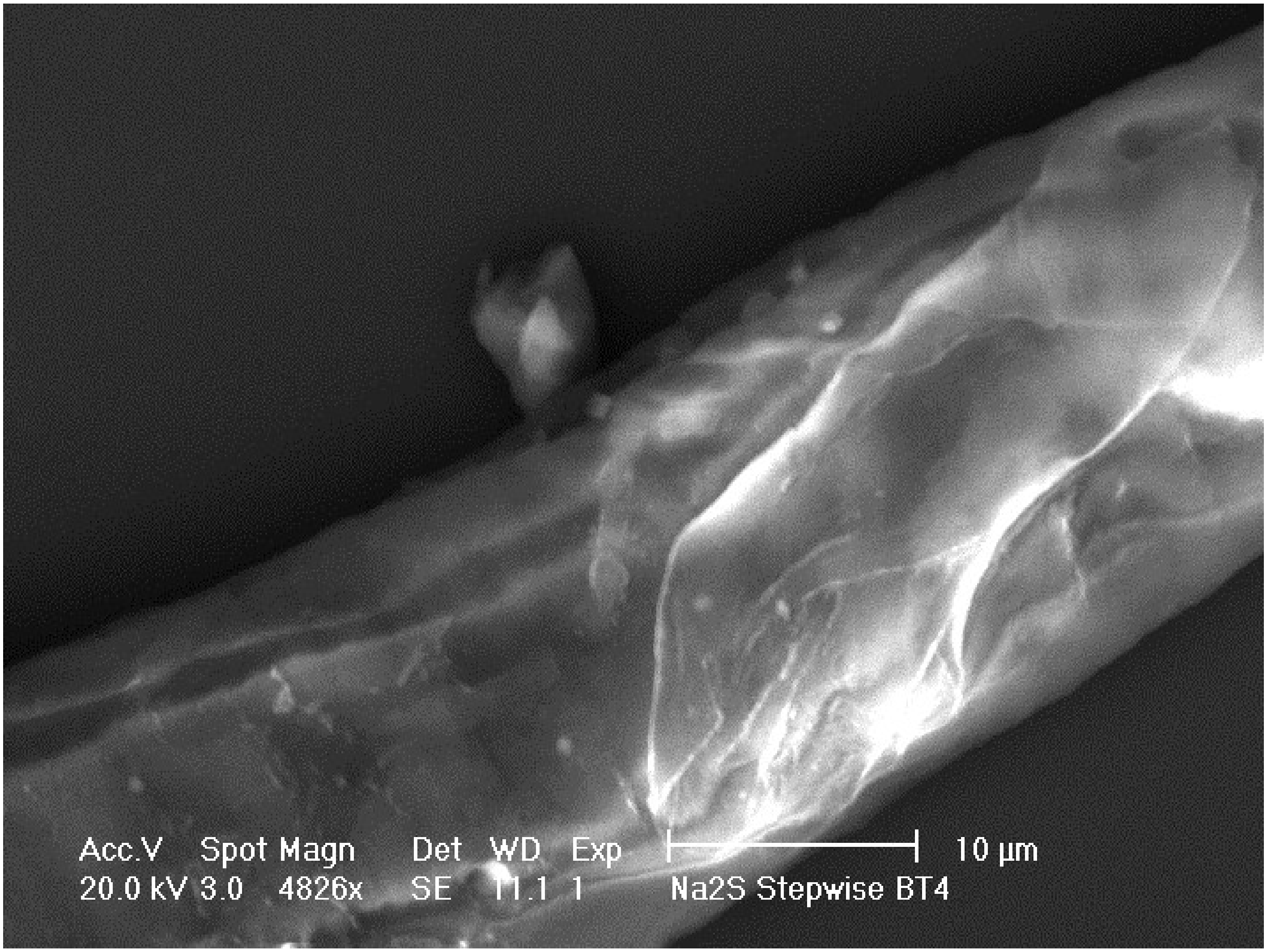

Figure S21. Scanning electron microscopy image of initially prepared **PDI-TEOAm-C_2OH** assembly drop casted on a silicon solid-state substrate from H_2O solution.

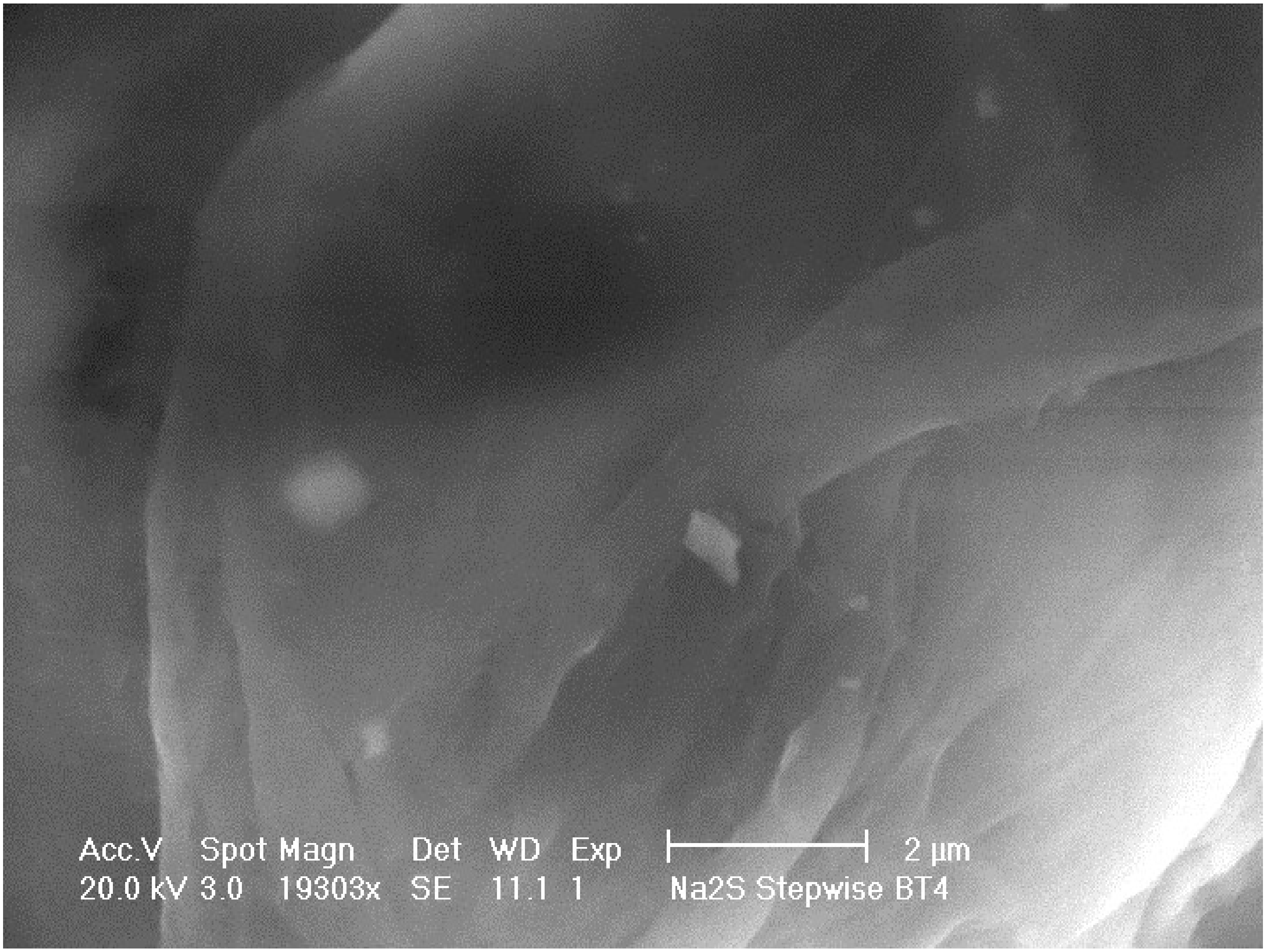

Figure S22. Scanning electron microscopy image of initially prepared **PDI-TEOAm-C_2OH** assembly drop casted on a silicon solid-state substrate from H_2O solution.

7. Nuclear Magnetic Resonance, ElectroSpray Ionization Mass, and Infrared Spectra – Figure S22 to S42

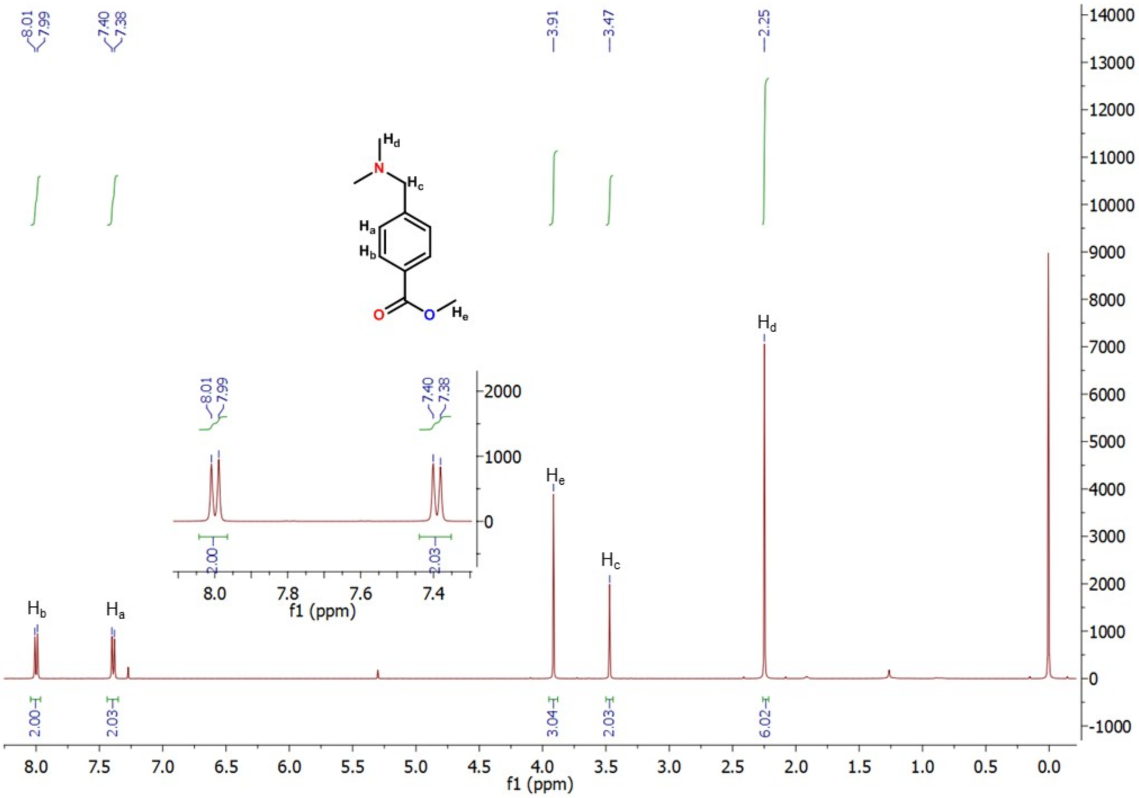

Figure S23. ^{1}H NMR spectrum (400 MHz, $CDCl_3$, 298 K) of **1**.

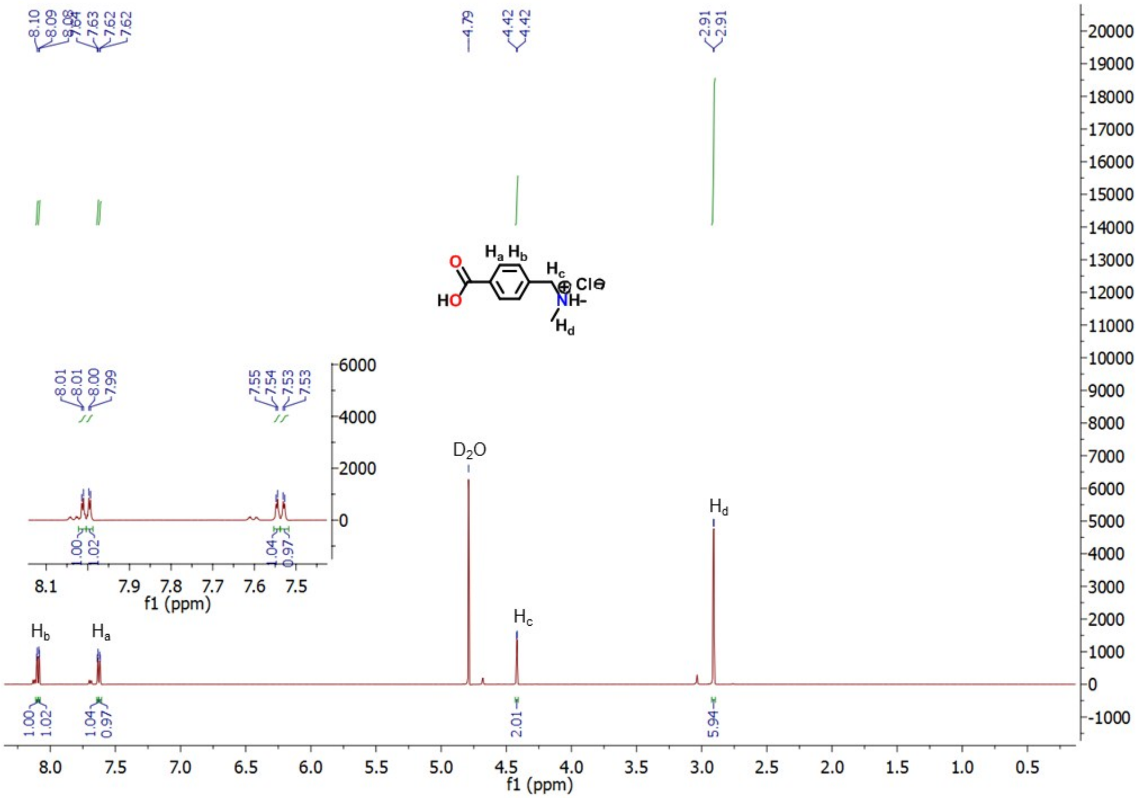

Figure S24. ^{1}H NMR spectrum (500 MHz, D_2O, 298 K) of **2**.

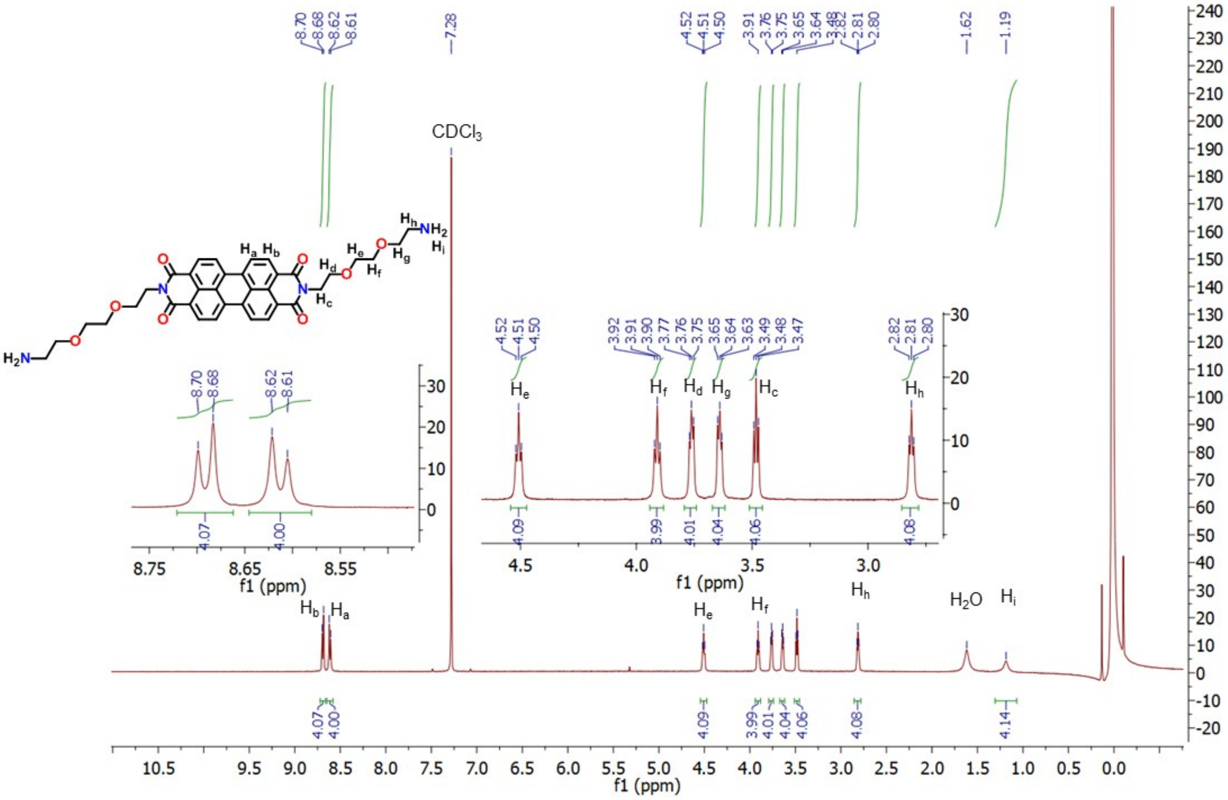

Figure S25. ^{1}H NMR spectrum (500 MHz, $CDCl_3$/MeOD (30:1, *v/v*), 298 K) of **PDI-TEO**.

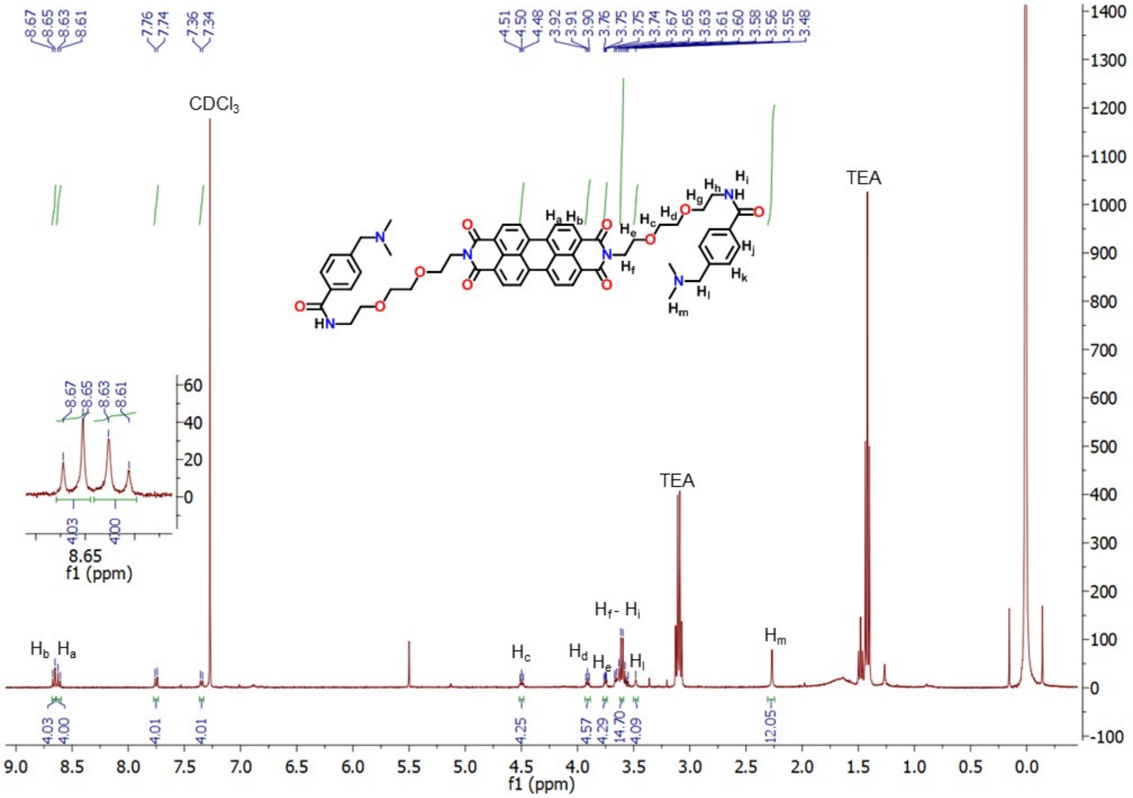

Figure S26. ^{1}H NMR spectrum (400 MHz, $CDCl_3$/MeOD (30:1, *v/v*), 298 K) of **PDI-TEOAm**.

Figure S27. ^{1}H NMR spectrum (400 MHz, d_6-DMSO, 298 K) of **PDI-TEOAm-C$_2$OH**.

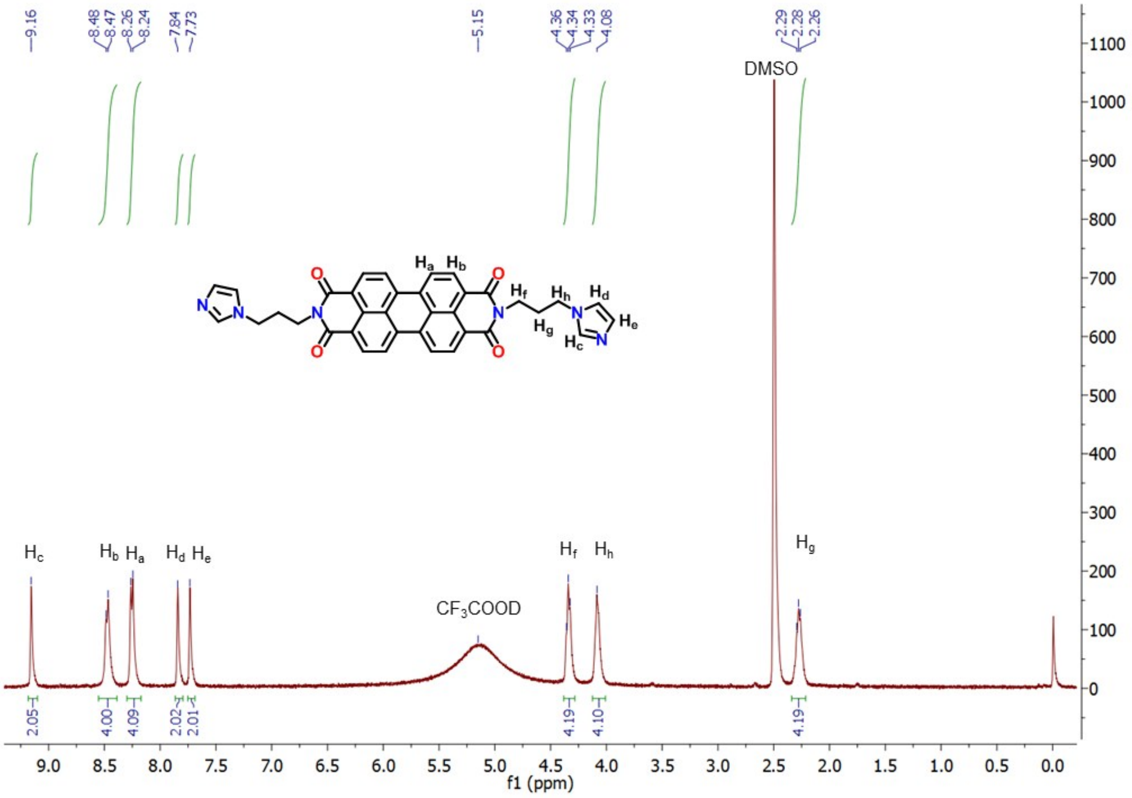

Figure S28. ^{1}H NMR spectrum (400 MHz, d_6-DMSO/CF_3COOD (30:1, *v/v*), 298 K) of **PDI-C$_3$Im**.

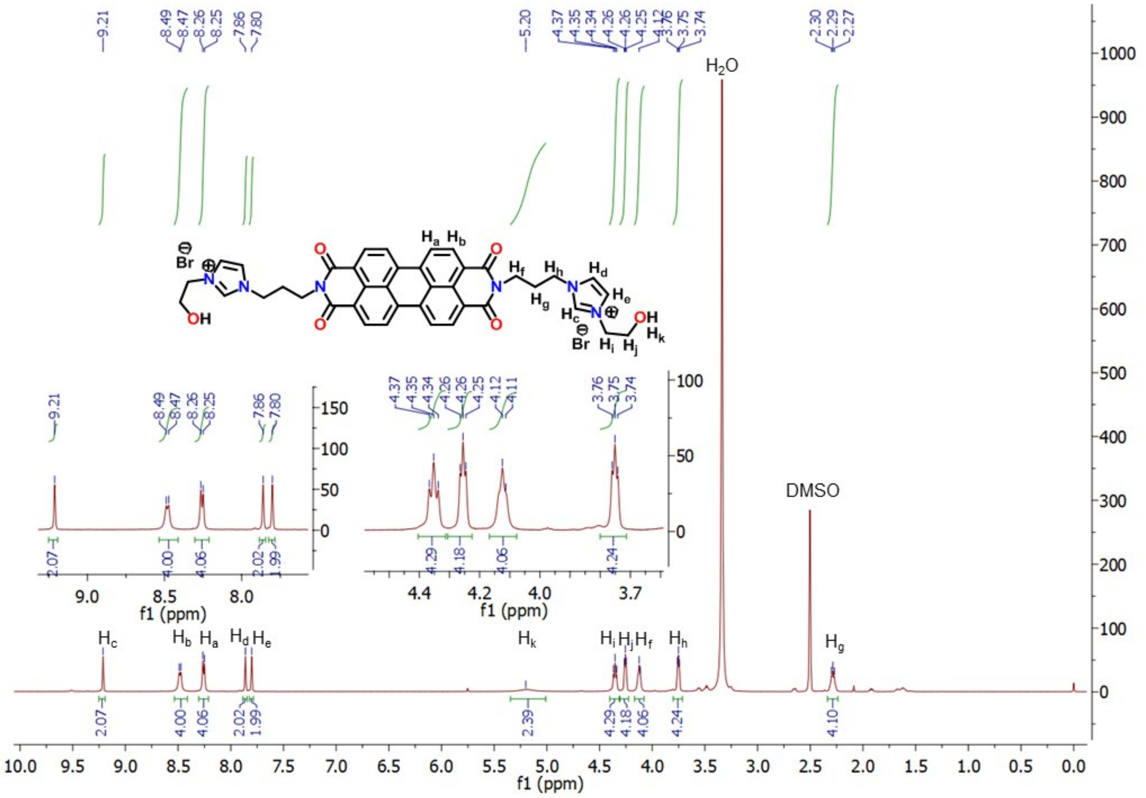

Figure S29. ^{1}H NMR spectrum (500 MHz, d_6-DMSO, 298 K) of **PDI-C$_3$Im-C$_2$OH**.

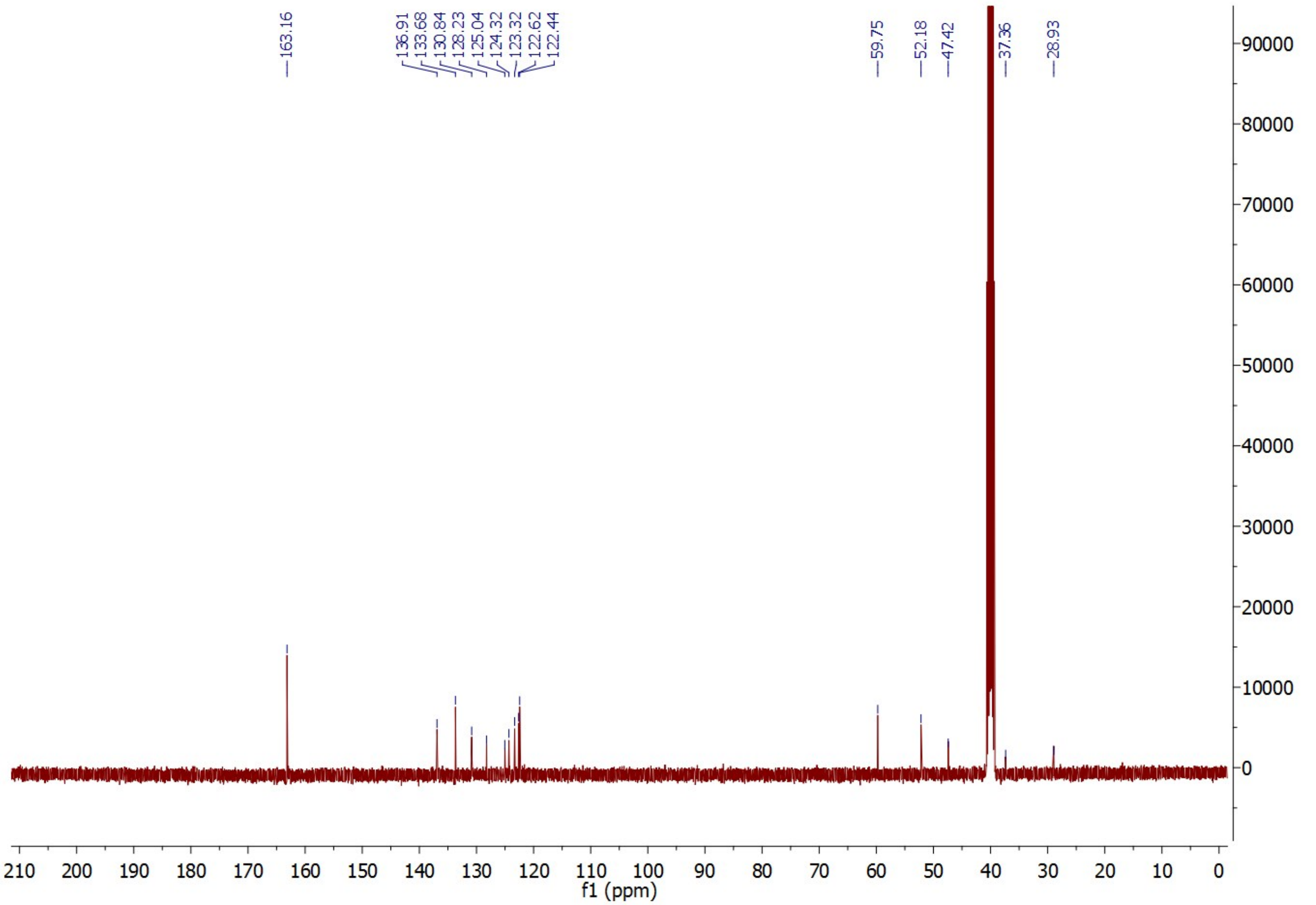

Figure S30. ^{13}C NMR spectrum (101 MHz, d_6-DMSO, 298 K) of **PDI-C$_3$Im-C$_2$OH**.

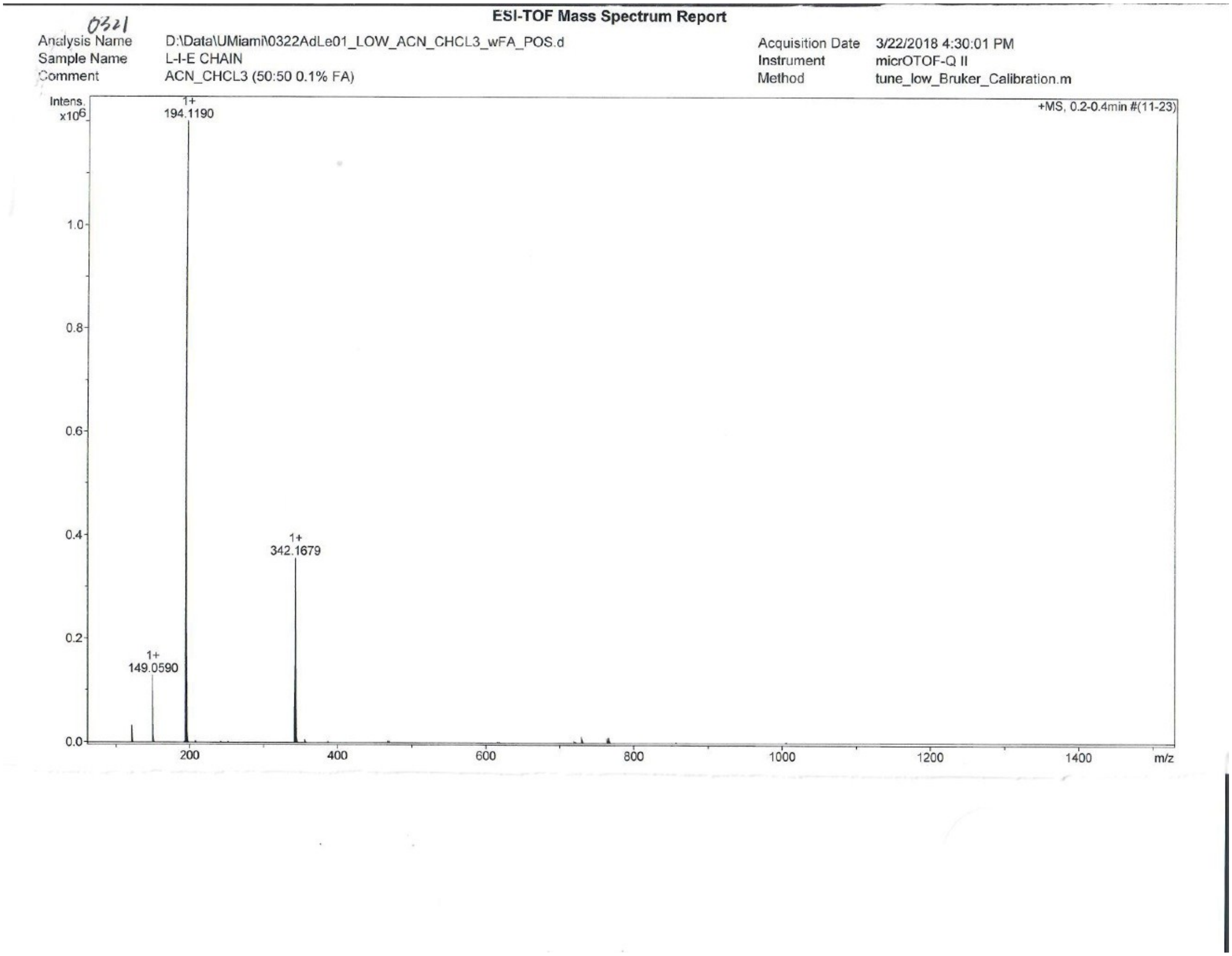

0321

ESI-TOF Mass Spectrum Report

Analysis Name D:\Data\UMiami\0322AdLe01_LOW_ACN_CHCL3_wFA_POS.d
Sample Name L-I-E CHAIN
Comment ACN_CHCL3 (50:50 0.1% FA)

Acquisition Date 3/22/2018 4:30:01 PM
Instrument micrOTOF-Q II
Method tune_low_Bruker_Calibration.m

Figure S31. High-resolution mass spectrum (ESI) of **1**.

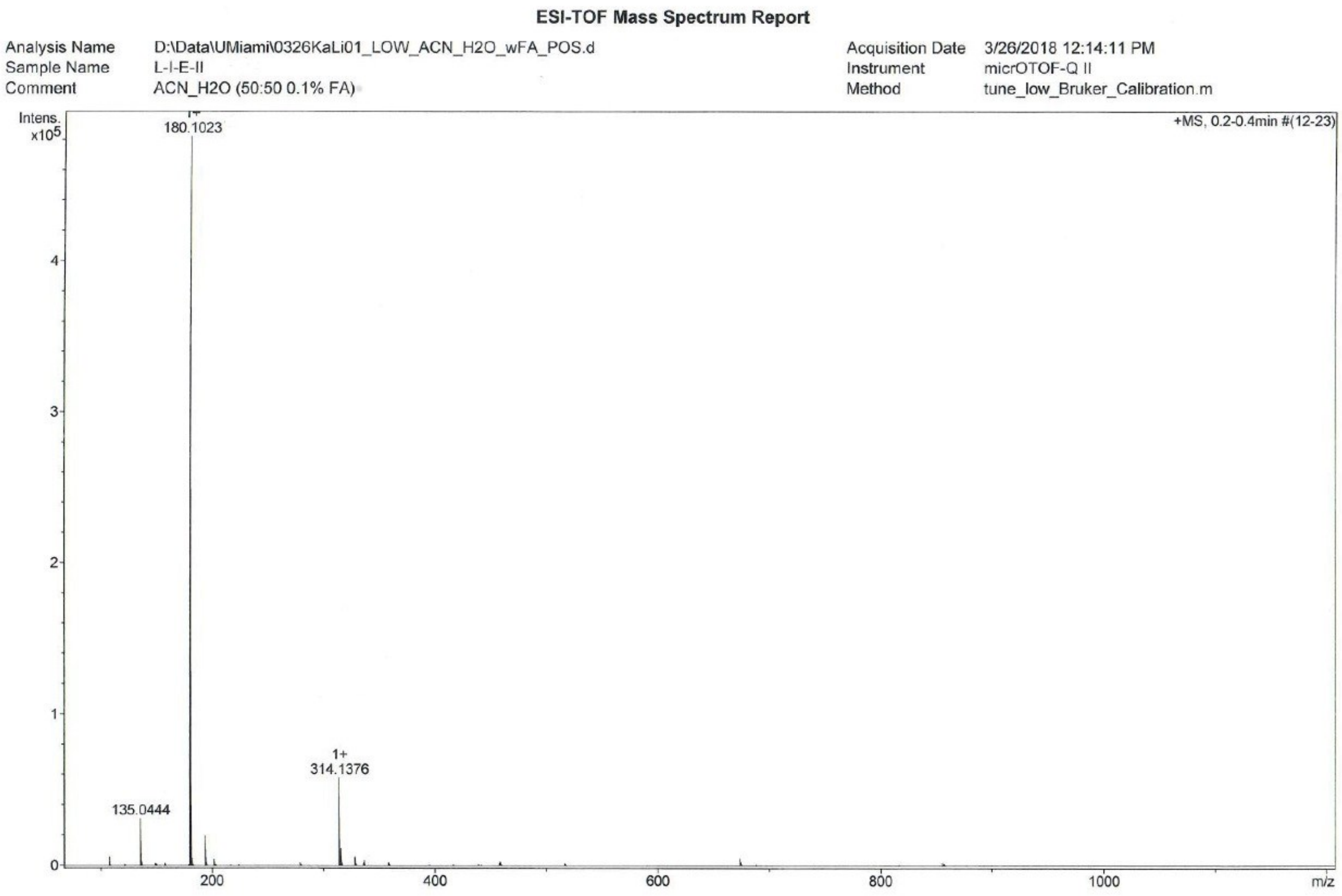

ESI-TOF Mass Spectrum Report

Analysis Name D:\Data\UMiami\0326KaLi01_LOW_ACN_H2O_wFA_POS.d
Sample Name L-I-E-II
Comment ACN_H2O (50:50 0.1% FA)

Acquisition Date 3/26/2018 12:14:11 PM
Instrument micrOTOF-Q II
Method tune_low_Bruker_Calibration.m

Figure S32. High-resolution mass spectrum (ESI) of **2**.

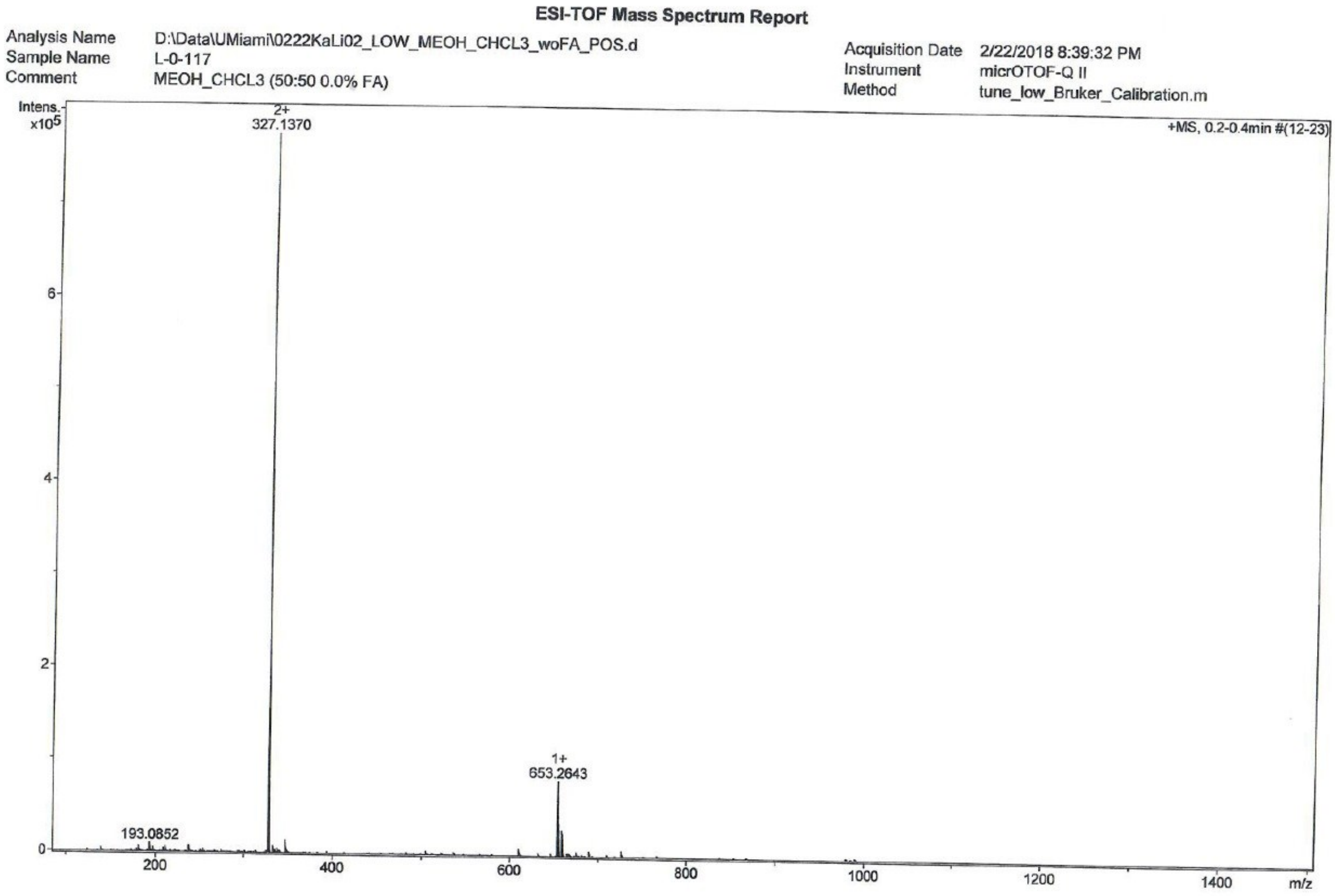

ESI-TOF Mass Spectrum Report

Analysis Name D:\Data\UMiami\0222KaLi02_LOW_MEOH_CHCL3_woFA_POS.d
Sample Name L-0-117
Comment MEOH_CHCL3 (50:50 0.0% FA)

Acquisition Date 2/22/2018 8:39:32 PM
Instrument micrOTOF-Q II
Method tune_low_Bruker_Calibration.m

Figure S33. High-resolution mass spectrum (ESI) of **PDI-TEO**.

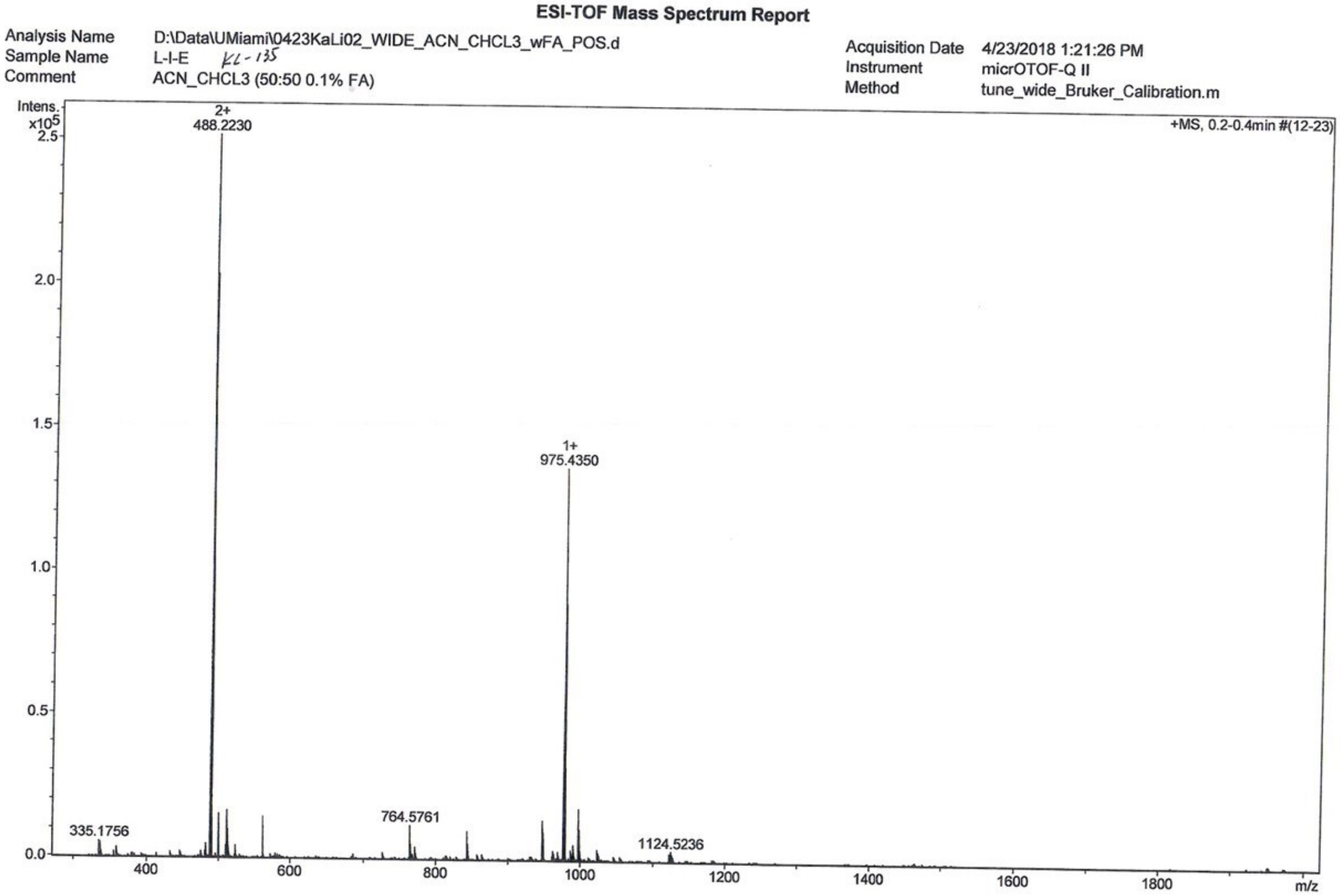

ESI-TOF Mass Spectrum Report

Analysis Name D:\Data\UMiami\0423KaLi02_WIDE_ACN_CHCL3_wFA_POS.d
Sample Name L-I-E KL-135
Comment ACN_CHCL3 (50:50 0.1% FA)
Acquisition Date 4/23/2018 1:21:26 PM
Instrument micrOTOF-Q II
Method tune_wide_Bruker_Calibration.m

Figure S34. High-resolution mass spectrum (ESI) of **PDI-TEOAm**.

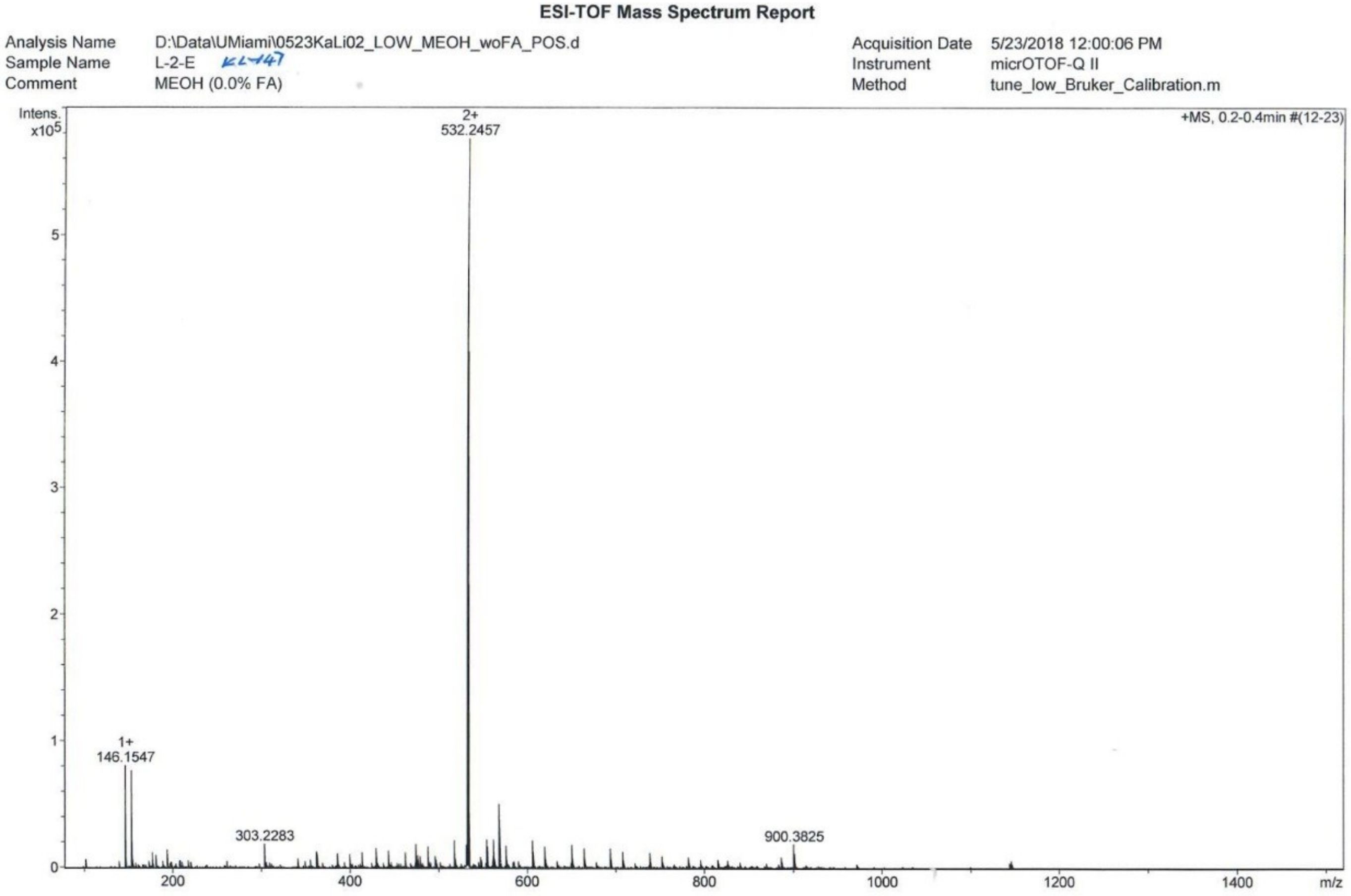

ESI-TOF Mass Spectrum Report

Analysis Name D:\Data\UMiami\0523KaLi02_LOW_MEOH_woFA_POS.d
Sample Name L-2-E KL-147
Comment MEOH (0.0% FA)
Acquisition Date 5/23/2018 12:00:06 PM
Instrument micrOTOF-Q II
Method tune_low_Bruker_Calibration.m

Figure S35. High-resolution mass spectrum (ESI) of **PDI-TEOAm-C$_2$OH**.

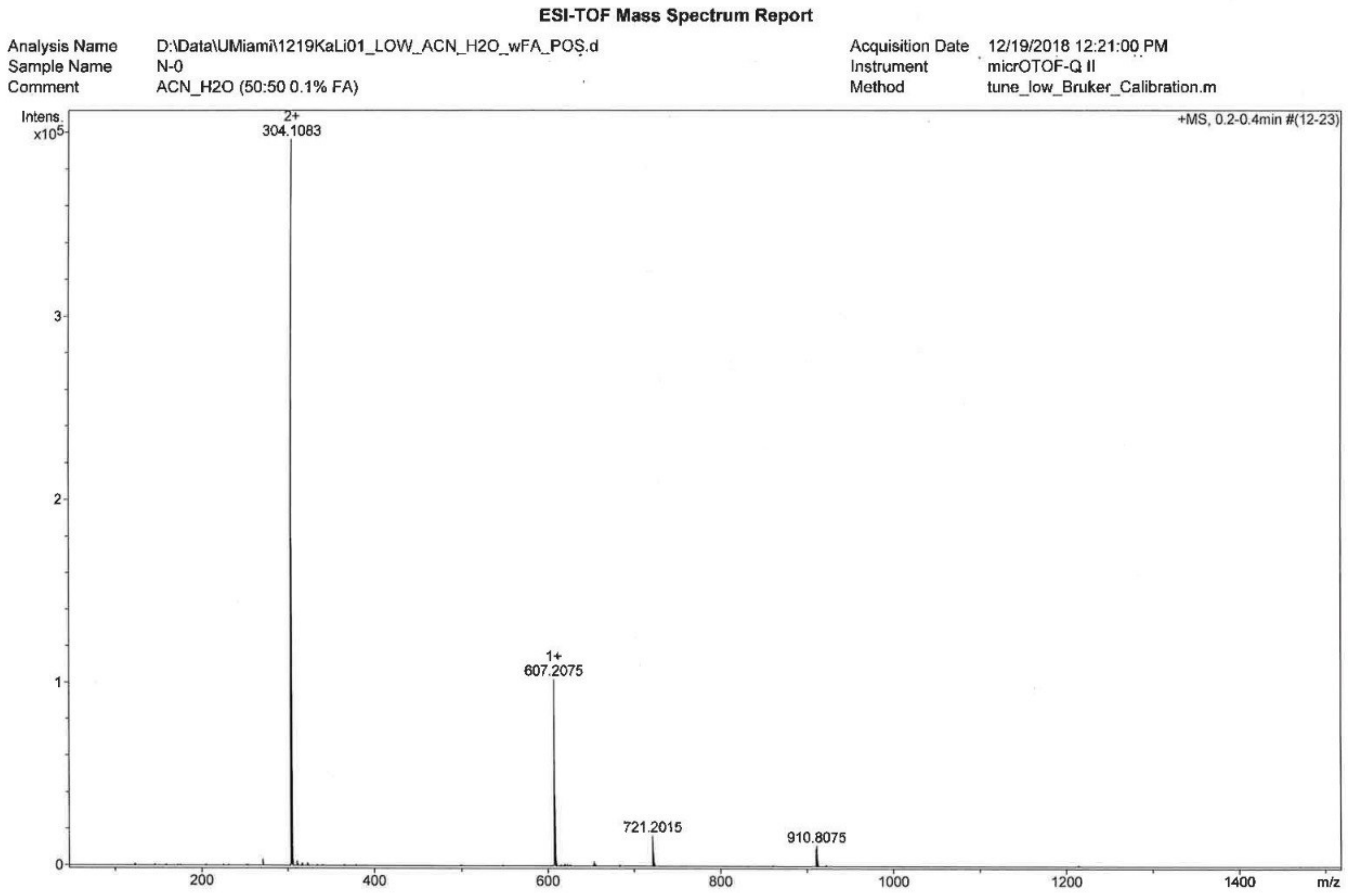

ESI-TOF Mass Spectrum Report

Analysis Name D:\Data\UMiami\1219KaLi01_LOW_ACN_H2O_wFA_POS.d
Sample Name N-0
Comment ACN_H2O (50:50 0.1% FA)

Acquisition Date 12/19/2018 12:21:00 PM
Instrument micrOTOF-Q II
Method tune_low_Bruker_Calibration.m

Figure S36. High-resolution mass spectrum (ESI) of **PDI-C$_3$Im**.

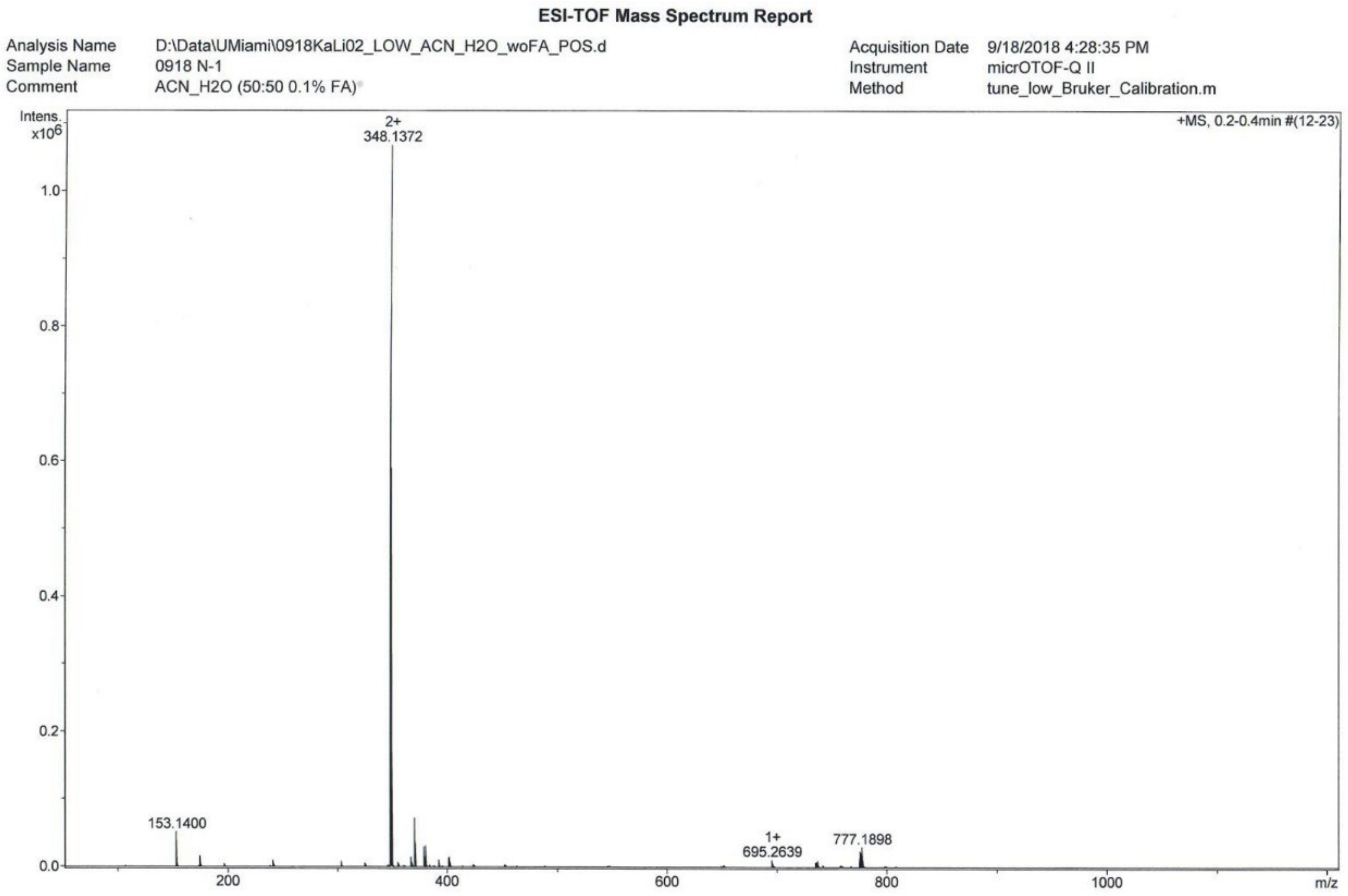

ESI-TOF Mass Spectrum Report

Analysis Name D:\Data\UMiami\0918KaLi02_LOW_ACN_H2O_woFA_POS.d
Sample Name 0918 N-1
Comment ACN_H2O (50:50 0.1% FA)

Acquisition Date 9/18/2018 4:28:35 PM
Instrument micrOTOF-Q II
Method tune_low_Bruker_Calibration.m

Figure S37. High-resolution mass spectrum (ESI) of **PDI-C_3Im-C_2OH**.

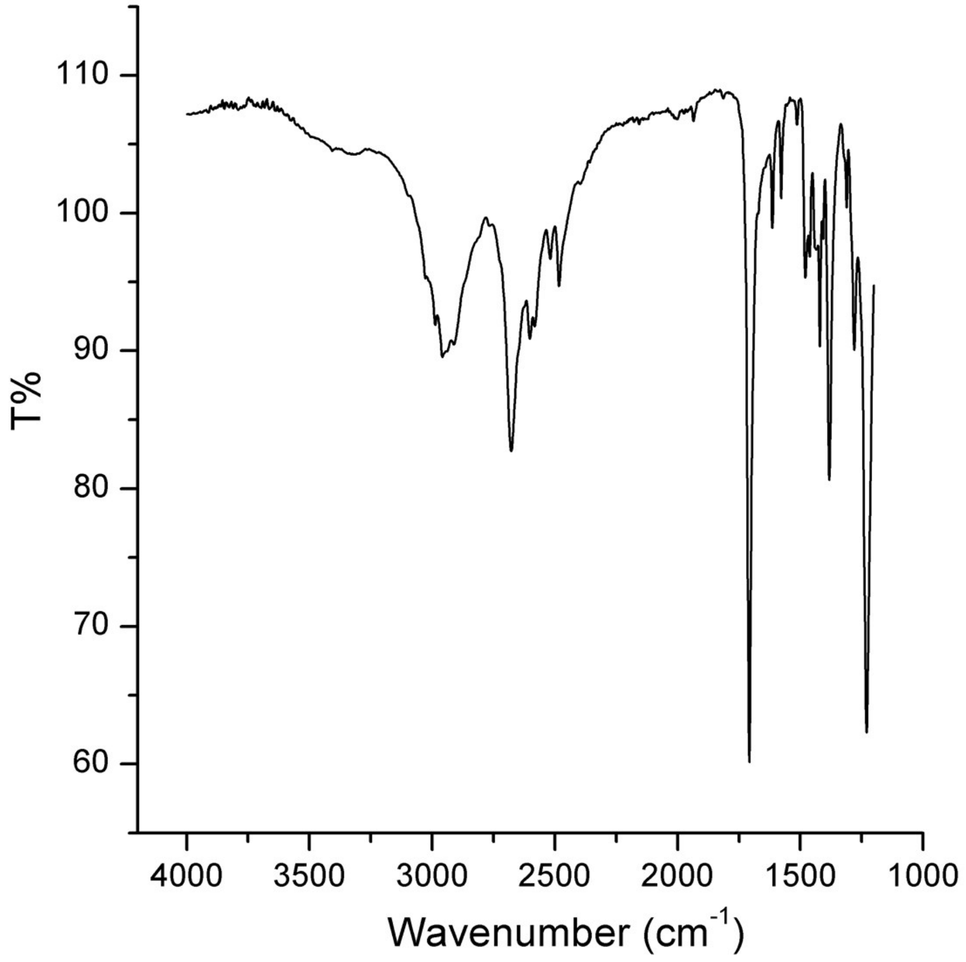

Figure S38. FTIR spectrum (neat solid) of **2**.

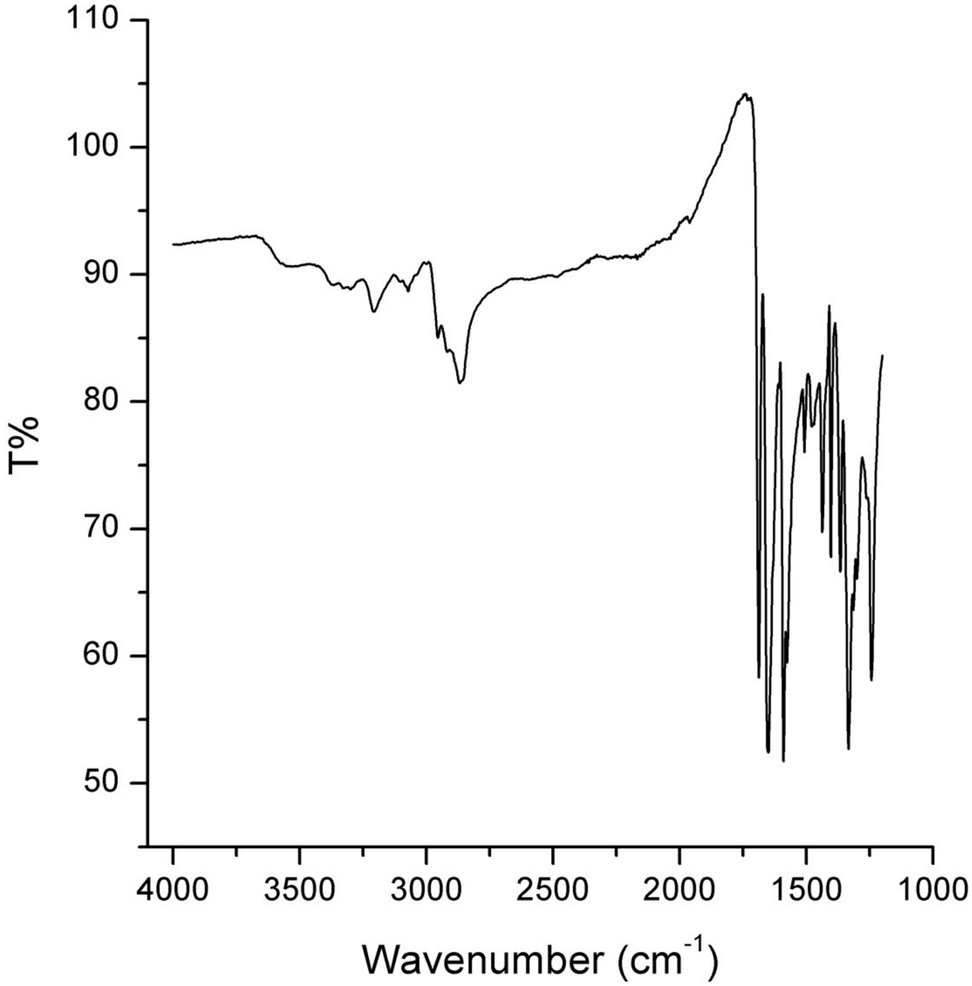

Figure S39. FTIR spectrum (neat solid) of **PDI-TEO**.

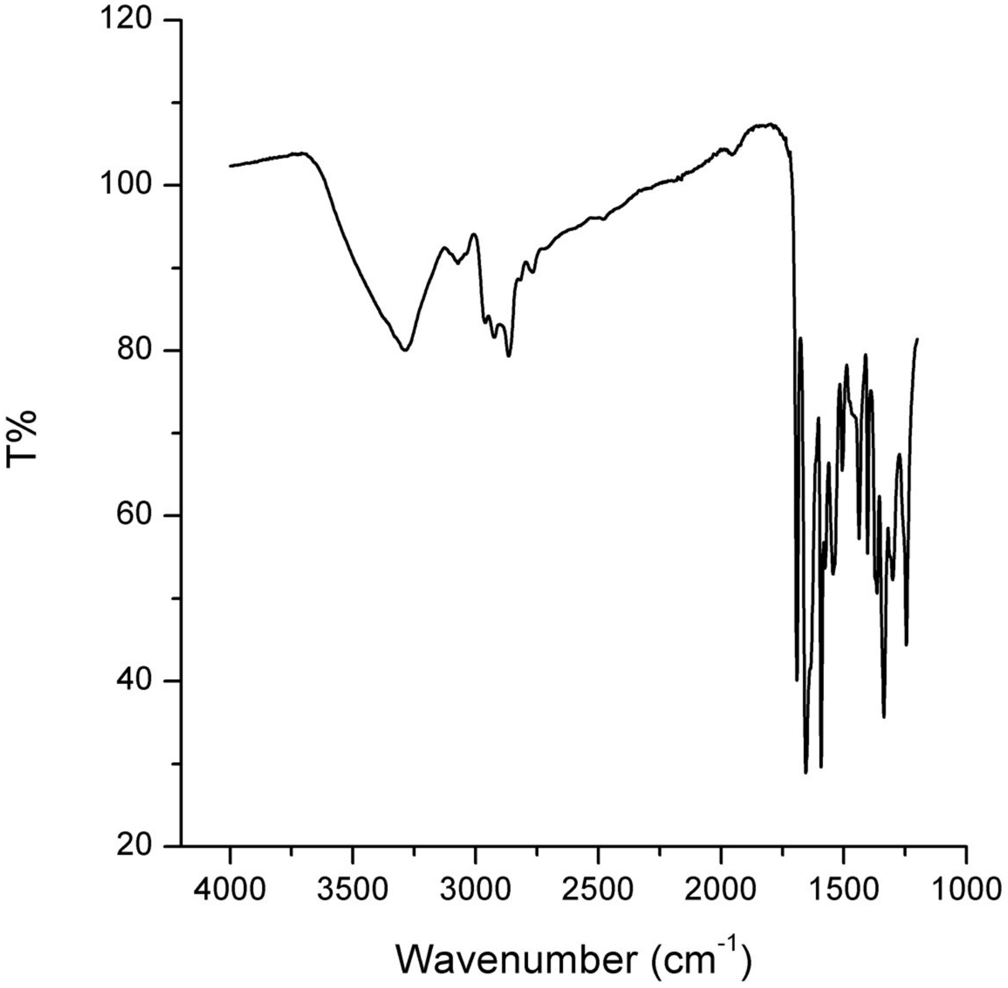

Figure S40. FTIR spectrum (neat solid) of **PDI-TEOAm**.

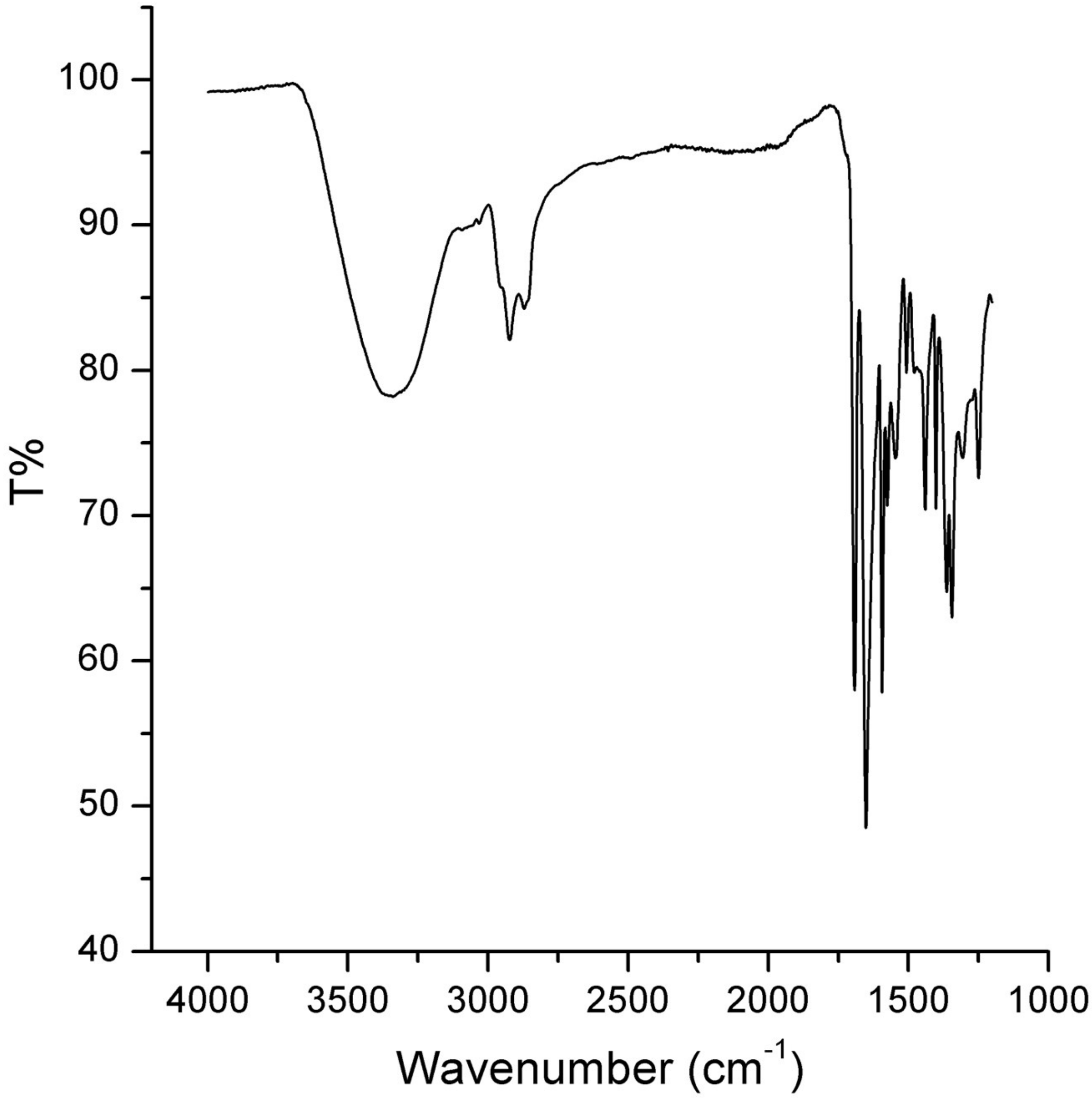

Figure S41. FTIR spectrum (neat solid) of **PDI-TEOAm-C_2OH**.

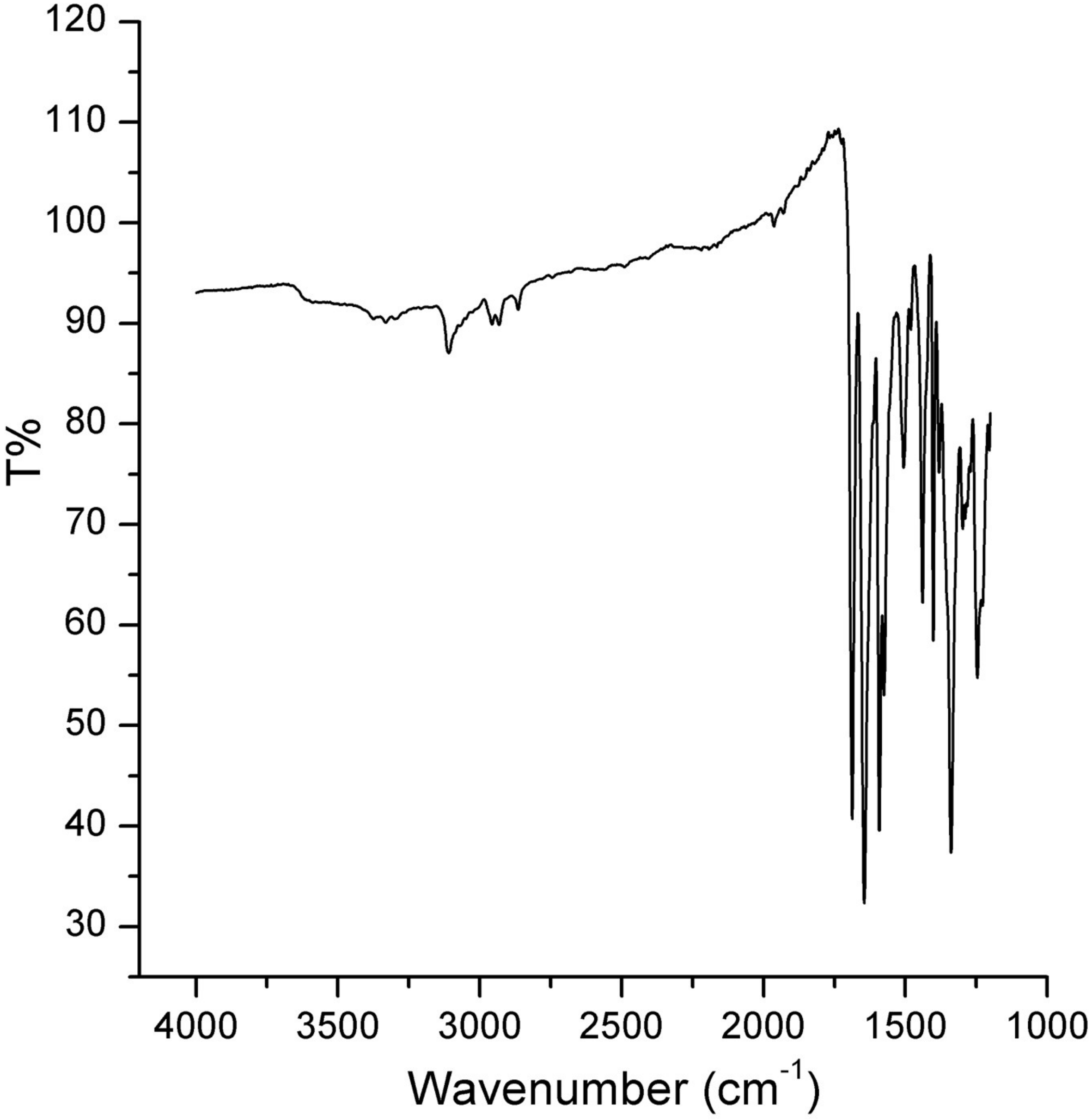

Figure S42. FTIR spectrum (neat solid) of **PDI-C$_3$Im**.

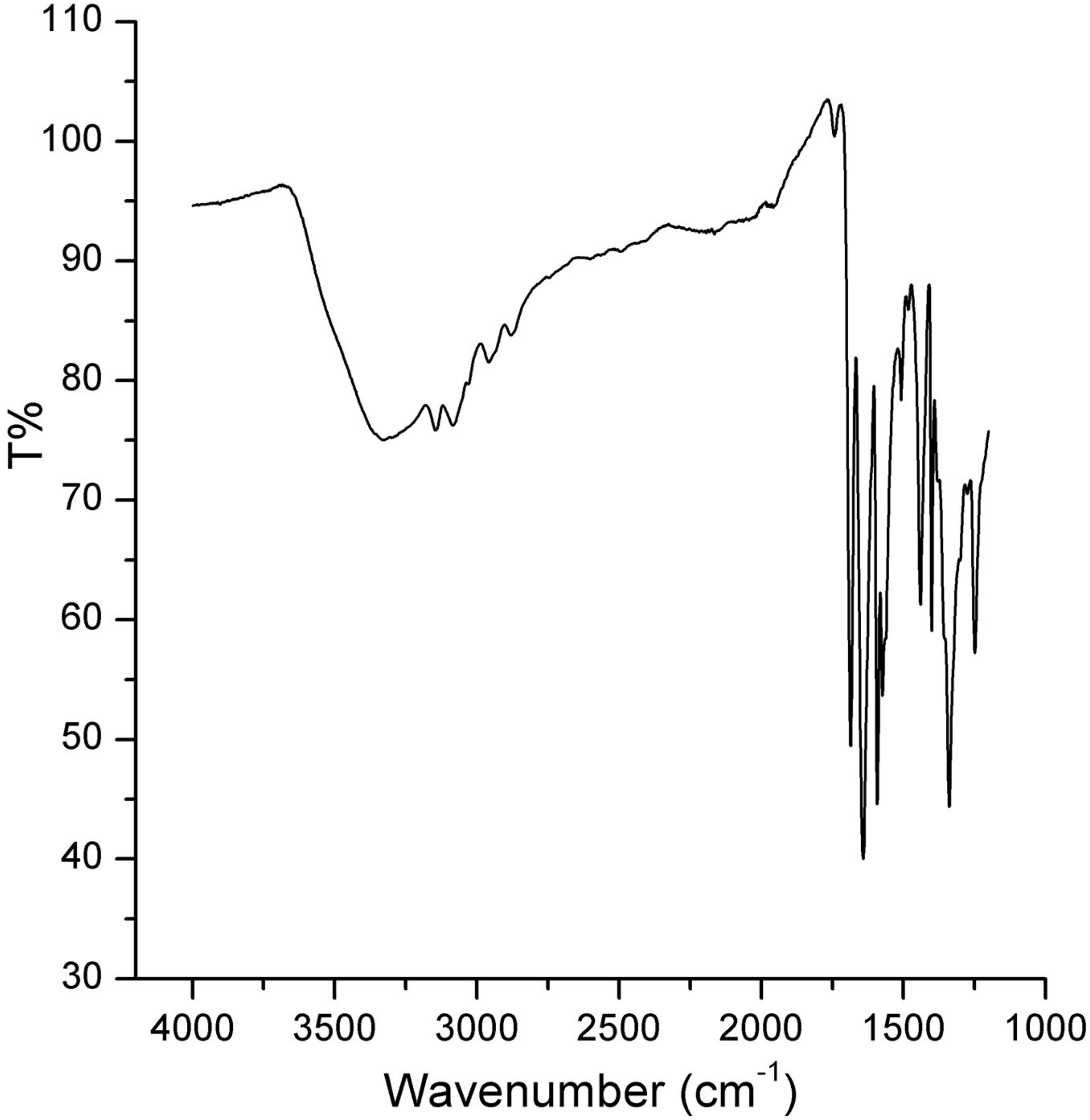

Figure S43. FTIR spectrum (neat solid) of **PDI-C_3Im-C_2OH**.

8. References

1. Williams, D. B. G.; Lawton, M., Drying of Organic Solvents: Quantitative Evaluation of the Efficiency of Several Desiccants. *J. Org. Chem.* **2010**, *75*, 8351-8354.
2. Horiuchi, T.; Nagata, M.; Kitagawa, M.; Akahane, K.; Uoto, K., Discovery of novel thieno[2,3-d]pyrimidin-4-yl hydrazone-based inhibitors of cyclin D1-CDK4: synthesis, biological evaluation and structure-activity relationships. Part 2. *Bioorg Med Chem* **2009**, *17*, 7850-7860.
3. Marcon, R. O.; Brochsztain, S., Aggregation of 3,4,9,10-Perylenediimide Radical Anions and Dianions Generated by Reduction with Dithionite in Aqueous Solutions. *J. Phys. Chem. A* **2009**, *113*, 1747-1752.
4. D'Anna, F.; Marullo, S.; Lazzara, G.; Vitale, P.; Noto, R., Aggregation Processes of Perylene Bisimide Diimidazolium Salts. *Chemistry* **2015**, *21*, 14780-14790.
5. Ogi, S.; Sugiyasu, K.; Manna, S.; Samitsu, S.; Takeuchi, M., Living supramolecular polymerization realized through a biomimetic approach. *Nat. Chem.* **2014**, *6*, 188-190.
6. Smulders, M. M. J.; Nieuwenhuizen, M. M. L.; de Greef, T. F. A.; van der Schoot, P.; Schenning, A. P. H. J.; Meijer, E. W., How to Distinguish Isodesmic from Cooperative Supramolecular Polymerisation. *Chem. Eur. J.* **2010**, *16*, 362-367.
7. Spano, F. C.; Silva, C., H- and J-Aggregate Behavior in Polymeric Semiconductors. *Annu. Rev. Phys. Chem.* **2014**, *65*, 477-500.
8. Spano, F. C., Absorption in regio-regular poly(3-hexyl)thiophene thin films: Fermi resonances, interband coupling and disorder. *Chem. Phys.* **2006**, *325*, 22-35.